



A comparative study on a complex URM building: part I—sensitivity of the seismic response to different modelling options in the equivalent frame models

Daria Ottonelli¹ · Carlo Filippo Manzini² · Corrado Marano³ · Emilia Angela Cordasco⁴ · Serena Cattari¹ 

Received: 17 January 2021 / Accepted: 13 May 2021 / Published online: 31 May 2021
© The Author(s) 2021

Abstract

The paper presents the comparison of the results of nonlinear static analyses carried out using six software packages (SWs) available at professional level and operating in the field of the equivalent frame (EF) approach on a model representative of a complex masonry building. The structure is inspired by the school “P. Capuzi” in Visso (MC, Italy), proposed as one of the benchmark structures in the “*URM nonlinear modelling—Benchmark project*” funded by the Italian Department of Civil Protection within the context of the ReLUIs projects. The 2-stories building is characterized by an irregular T-shaped plan and load-bearing walls consisting of two-leaf stone masonry with a rather regular bond scheme. The school was severely damaged by the seismic sequence that hit Central Italy in 2016/2017 and essentially exhibited a global in-plane box-type response, with a clear evidence of cracks concentrated in piers and spandrels. The availability of an accurate survey of the crack extension represents a precious and rare reference to firstly address in the paper the rules to be adopted in the EF models for the definition of the structural elements geometry. Then, the comparison of results is made with a twofold aim: firstly, by setting the models adopting shared and consistent modelling assumptions across the SWs; secondly, by investigating the sensitivity of the seismic response to some common epistemic and modelling uncertainties (namely: the adoption of various EF idealization rules for walls, the out-of-plane contribution of piers, the flange effect). In both cases, results are post-processed to define reference values of the achievable dispersion. The comparison is carried out in relation to a wide set of parameters, namely: global parameters (e.g. dynamic properties, pushover curves and equivalent bilinear curves); synthetic parameters of the structural safety (i.e. the maximum acceleration compatible with the ultimate limit state); the damage pattern simulated by SWs.

Keywords Benchmark structures · Comparative study · Masonry · Equivalent frame modelling · Nonlinear static analysis · Epistemic and modelling uncertainties

✉ Serena Cattari
serena.cattari@unige.it

Extended author information available on the last page of the article

1 Introduction

The comparative studies, available in literature and addressed to the modelling of unreinforced (URM) buildings, document a large scattering of achievable results, especially when used to finalize the seismic assessment through nonlinear analyses. This is mostly due to the too many possible choices in defining the numerical model and in interpreting the results. As evidence of this, the challenging topic is highlighted by both: research works specifically addressed to test different modelling strategies (e.g. Salonikios et al. 2003; Giamundo et al. 2014; Betti et al. 2014), considering also commercial software packages (e.g. Marques and Lourenco 2011; 2014; Calderoni et al. 2015; De Falco et al. 2017; Siano et al. 2018; Aşıkoğlu et al. 2020); or blind predictions involving a large number of research teams called to predict the seismic response of the same benchmark prototype (e.g. in Mendes et al. 2017; Esposito et al. 2019; Bartoli et al. 2017; Parisse et al. 2021).

Although unanimous in highlighting the huge potential scattering of achievable results, these comparative studies are not conclusive in quantifying the uncertainty associated to the software-to-software variability neither when used under the same hypotheses nor when the latter are kept free. Moreover, in most cases the aforementioned studies have been carried out on very simple structures (usually two-story single-unit or even single walls), using a quite limited number of software packages (SWs) (apart in the case of blind predictions) and focusing the comparison just on the pushover curves and the damage pattern. Actually, the comparison has been extended to local parameters—such as the evolution of internal generalized forces in specific structural elements—in very few cases, as in Marques and Lourenco (2014).

With the attempt to fill these gaps, a wide research program was carried out, starting in 2014, by several Italian Universities involved in the ReLUIs projects (*Rete dei Laboratori Universitari di Ingegneria Sismica*—Italian Network of University Seismic Laboratories), synthetically named in the following as "*URM nonlinear modelling—Benchmark project*" and described more in details in Cattari and Magenes (2021). In such a project, different benchmark examples of increasing complexity—ranging from the single panel to 3D existing buildings—have been specifically designed and analysed by a large set of SWs belonging to various modelling strategies. Moreover, detailed input data for all of the considered case studies, allowing them to be replicated also by other researchers and analysts, are provided in Cattari and Magenes (2021) as supplementary electronic material.

Within this context, the paper presents the comparative study carried out on the benchmark structure named BS5, inspired by the geometry and typological-constructive data of the "P. Capuzi" school in Visso (MC, Italy). This building was built in the 30 s and strengthened following the Umbria-Marche 1997 earthquake. It was severely damaged by the seismic sequence that affected Central Italy in 2016/2017, mainly exhibiting a global box-type behavior with cracks concentrated in piers and spandrels. The structure, now demolished because of the serious damage suffered, was the subject of a permanent seismic monitoring system by the DPC through the OSS (acronym of the Italian name "*Osservatorio Sismico delle Strutture*") (Dolce et al. 2017) and was analyzed in other literature works with the aim of an accurate numerical simulation of its actual response (Cattari et al. 2019; Graziotti et al. 2019; Ferrero et al. 2020; Brunelli et al. 2021).

Although this paper investigates this structure from a different perspective (i.e. a comparative rather than a validation study), nonetheless the availability of an accurate survey of the damage occurred provides very interesting data to support some modelling assumptions, such as the criteria adopted for the equivalent frame idealization of walls (as

illustrated in Sect. 2.1), and to carry out a comparison with the actual response in qualitative terms (e.g. damage pattern, as discussed in Sect. 3.4).

The paper focuses the attention on the results achieved by performing nonlinear static analyses through six SWs which work in the field of the equivalent frame (EF) modeling, also available at professional level, while the companion paper made by Castellazzi et al. (2021) investigates the same topic by adopting three additional SWs belonging to continuum and discrete-macroelement models (synthetically called as “refined models” in the following).

While other literature works already provided an in-depth state-of-the-art of the different options involved in the equivalent frame modelling process (Quagliarini et al. 2017) or a discussion on the repercussions of some of them in the seismic assessment (Rota et al. 2014; Bracchi et al. 2015; Cattari et al. 2021a; Manzini et al. 2021), in this paper the main objective is to quantify the dispersion of achievable results when using different SWs: firstly, by setting the models with shared and consistent modelling assumptions (Sect. 3); secondly, by investigating the sensitivity of the seismic response to some common epistemic and modelling uncertainties (Sect. 4). In particular, in Sect. 3 the comparison is made in terms of total masses, dynamic parameters (periods and modal shapes obtained from the execution of a modal analysis) and results from nonlinear static analyses (e.g. pushover curve, parameters of the equivalent bilinear curve and damage occurred in structural elements). In Sect. 4, the effect of alternative equivalent frame idealization criteria adopted for masonry walls, the role of the out-of-plane contribution of piers and different assumptions for the effectiveness of wall-to-wall connections are investigated by analyzing the abovementioned parameters representative of the global structural response.

Finally, in Sect. 5, passing to an engineering practice-oriented perspective, the repercussions of the dispersion of results on the seismic verification are discussed by computing the maximum peak ground acceleration (PGA) compatible with the attainment of the ultimate displacement capacity of the structure as estimated through the pushover curves.

2 Brief description of the benchmark case study and modelling hypotheses adopted

With respect to the original configuration of the “P. Capuzi” school, some simplifications have been introduced in the “*URM nonlinear modelling—Benchmark project*”, as accurately described in the Annex I-*Benchmark Structures Input Data* included as supplementary electronic material in Cattari and Magenes (2021). The latter contains also the complete set of input data necessary to reproduce the BS5 by other researchers, while in the following only the essential features are recalled.

In particular, the structure is on two levels plus an attic floor, this latter having been simulated in the analysis only in terms of equivalent mass; conversely, the underground part visible in Figs. 3, 4 and 5 has not been modelled, according to the simplifications introduced in the project. The BS has an irregular shape, assimilable to a T (Fig. 1), and is characterized by load-bearing unreinforced masonry and rigid floors. The walls are mainly made of cut stone masonry with good bonding (Cut stone in Fig. 1.a). Some walls have undergone strengthen interventions with mortar injections (Cut stone—S in Fig. 1a). Moreover, pillars and limited portions composed by a solid brick and mortar joints masonry (Brick in Fig. 1a) are present in a more sporadic way.

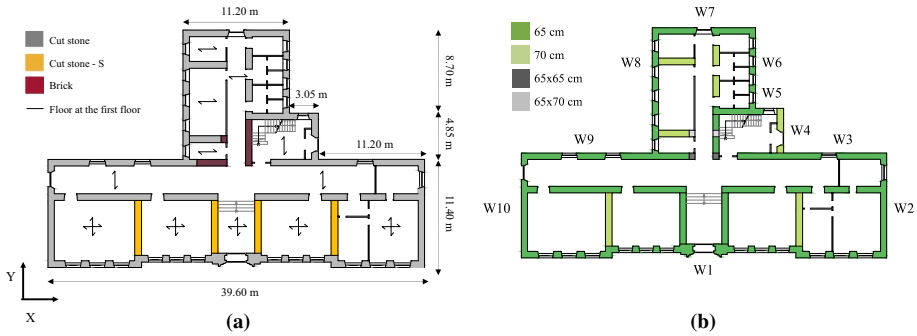


Fig. 1 **a** Identification of masonry types at the ground floor; **b** identification of wall thickness of the ground floor and numbering of the walls

In order to investigate the dispersion of the results achievable from different SWs also varying some structural details common in existing buildings, two different parametric configurations have been analyzed, namely:

- BS5/A—masonry spandrels not coupled to any tensile resistant horizontal element at floor level. In this case, only the presence of an effective lintel is assumed, while the contribution of other factors that can produce an equivalent tensile strength on spandrels (such as the interlocking with the adjacent masonry region, as discussed in Beyer and Mangalathu 2013) is neglected. This configuration aims to promote the so-called “weak spandrels” behavior.
- BS5/C—masonry spandrels coupled to reinforced concrete (r.c.) tie beams.

The analysis of cases BS5/A and BS5/C allows to extend to a complex building some considerations on the coupling role provided by spandrels to piers already emerged from the analysis of other simpler benchmark structures, like that analyzed in Manzini et al. (2021). The BS5/C case is the most consistent with the actual configuration of the building. In particular, since in-situ investigations detected the presence of a full thickness r.c. tie beam, the modelling hypothesis consisting of spandrels broken up at the level of the r.c. tie beam has been assumed. For simplicity, the same spandrels geometry has been adopted also in the case BS5/A.

To reduce the dispersion in the results, the following assumptions were shared among the Research Teams (RTs) involved in the “URM nonlinear modelling—Benchmark project”:

- The geometrical data (such as the wall thicknesses, as synthetically reported in Fig. 1b for the ground floor).
- The distribution and values of the floor loads, including that of the roof, considered only as an equivalent additional mass and not through the explicit modelling of each single structural element. Figure 1a depicts the main spanning orientation of diaphragms.
- The mechanical properties of all materials.

With regard to the materials properties, Table 1 summarizes the values adopted for the masonry types that characterize the building. The values are compatible with the reference range of variation proposed in the Instructions of the Italian Technical Standards (MIT 2019) for the corresponding analogous masonry types; the reliability of these values is confirmed also by other experimental literature data (e.g. Krzan et al. 2015; Vanin et al. 2017). Consistently with what usually recommended by Codes (e.g.: NTC (2018), EC8-3 (CEN 2005)), in order to reproduce the effects of progressing cracking, a reduction factor conventionally equal to 0.50 has been applied to the gross stiffness of each element. In this respect, it is noted that the values of the elastic moduli of masonry summarized in Table 1 refer to the initial elastic condition.

The parameters summarized in Table 1 have been adopted as target for a twofold aim: in the EF models discussed in this paper, to evaluate the shear strength associated to masonry elements according to the common criteria proposed in literature (Calderini et al. 2009); in the more refined models presented in the companion paper by Castellazzi et al. (2021), to calibrate the more complex set of parameters which the constitutive laws adopted by the refined models are based on. The latter process is essential to guarantee a cross-consistency among models belonging to different modelling approaches working at different scales (as discussed in-depth also in D’Altri et al. 2021 and in Cattari et al. 2021b).

In particular, in the equivalent frame models, the strength associated with the flexural failure mode of piers is evaluated by neglecting the tensile strength of the material and assuming at the compressed toe an equivalent rectangular stress block of normal stresses of height $0.85 f_m$ (where f_m is the compressive strength of masonry and 0.85 is the stress-block equivalence coefficient, as proposed in NTC (2018) and EC8-3 (CEN 2005)). In the case of the spandrels, the flexural behavior is differently interpreted in cases BS5/A and BS5/C. For the BS5/C case, the development of a strut mechanism was assumed likely to occur due to the presence of r.c. tie beams and it was interpreted according to the criterion proposed in NTC (2018), considering the maximum normal stress transmissible by the tensile resistant element coupled to the spandrel. Conversely, in the BS5/A case, among the different options (see Beyer and Manalaghu 2013; Betti et al. 2008), the same criterion adopted for piers has been assumed that, on the safe side, presupposes to neglect any possible contribution of an equivalent tensile strength of spandrel generated at the end section by the interlocking effects with the adjacent masonry portions. Such an assumption produces in the BS5/A case an almost negligible flexural strength of spandrel, that in fact has been directly considered null by the RT that used SW7, by modelling the spandrels as axially rigid rod elements, coupling piers only for the horizontal displacements.

For the computation of the strength associated to the shear failure mode of both piers and spandrels, the criterion proposed by Turnšek and Cačovic (1971), aimed to interpret the diagonal shear failure mode, has been assumed with the modification introduced in Turnšek and Sheppard (1980).

Table 1 Mechanical parameters adopted for BS5

Masonry typology	f_m (N/mm ²)	τ_0 (N/mm ²)	E (N/mm ²)	G (N/mm ²)	w (kN/m ³)
Cut stone	3.20	0.065	1740	580	21
Strengthen (S)	4.8	0.0975	2610	870	
Solid brick (medium times 1.5)	4.8	0.114	2250	750	18

f_m = compressive strength; τ_0 = masonry shear strength; E = Young modulus (vertical direction); G = shear modulus; w = specific weight

In the following sections, the comparison of the results of the non-linear static analyses performed by six different SWs belonging to the EF approach are presented and commented. All of them describe the response of the structural elements through non-linear frame elements with “zero-length” lumped plasticity. For masonry elements, a bi-linear elastic perfectly plastic constitutive law with a limitation of the maximum (ultimate) displacement in terms of drift threshold is assumed. The strength is computed as the minimum between the shear and flexural strength criteria afore described, while, for the drift, the limit values equal to 0.4% and 0.6% have been assumed for the shear and the flexural failure modes, respectively. In particular, the following SWs, available also at professional and commercial level, have been used (see Fig. 2 for a 3D view of corresponding numerical models):

- 3Muri (2016, release 10.0.1), based on the solver developed by Lagomarsino et al. 2013 and distributed by S.T.A. DATA.
- Aedes.PCM (2017), based on the hinge formulation proposed in Spacone and Camata (2007) and distributed by Aedes.
- 2Si (2020) PRO_SAM Program (release 20.7.0), based on the SAM-II solver developed by Magenes et al. 2006 and distributed by 2Si. Actually, in the first years of the project the software ANDILWall (release 3.1.0.0, Manzini et al. 2006) was used that, nowadays no longer distributed, has then been replaced by Pro_SAM.
- CDSWin OpenSees (2016), distributed by STS.
- MIDAS Gen (2017), distributed by MIDAS Information Technology Co.
- SAP 2000 (2016, release 18), distributed by Computers and Structures Inc.

The results of the SWs are presented in the paper in anonymous way, tagging each software package through a number assigned in a random way in the “*URM nonlinear modelling—Benchmark project*”. A subset of the adopted SWs is compared in this paper; in particular, they are named as follows: SW1, SW2, SW3, SW5, SW6 and SW7. The choice

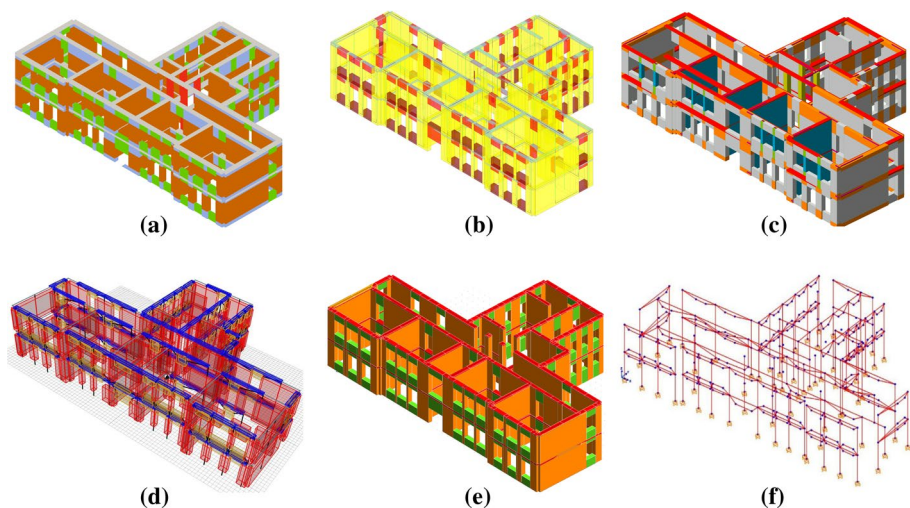


Fig. 2 3D views of the numerical models adopted in the research set through the following SWs: **a** 3Muri; **b** AEDES; **c** MIDAS Gen; **d** ANDILWALL (now 2Si); **e** CDSWin; **f** SAP 2000

to adopt an anonymous format is consistent with the overall scope of the project, that was not to express a judgment on the reliability of each specific software package but to provide a critical examination of the achievable results and the obtained differences.

In Sect. 3, in addition to the shared criteria previously discussed on the strength criteria and mechanical parameters, the following common assumptions have been adopted:

- Idealization in equivalent frame of the walls according to the criterion proposed in Lagomarsino et al. (2013).
- Full effective wall-to-wall connection.
- Neglected contribution of the out-of-plane stiffness and strength of piers.
- Rigid diaphragms.

2.1 Equivalent frame idealization criteria adopted for the URM walls

In the following (from Figs. 3, 4 and 5) the equivalent frame idealization compatible to the application of the most common criteria proposed in the literature and adopted in the professional practice is reported as an example for some of the façades (W6, W8 and W10, as numbered in Fig. 1b). In particular, the investigated criteria are: (a) Lagomarsino et al. (2013), (b) Augenti (2006), (c) Dolce (1991) and (d) Moon et al. (2006). The criteria proposed in Dolce (1991) and Lagomarsino et al. (2013) start from the evidence of the observed damage integrated by numerical studies and comparisons with more accurate finite element simulations. The other two are derived empirically from the observation of experimental results (Moon et al. 2006) or from the past earthquakes damage (Augenti 2006). An important difference to recall is that, according to these two latter criteria, the pier effective height is a function of the direction of the seismic action; therefore, in these cases two different structural models have to be considered, depending on the direction of the performed analysis (positive or negative).

In the following Figures (from Figs. 3, 4 and 5) the pier effective height resulting from the different criteria (marked in red, for the positive direction, and yellow, for the negative direction

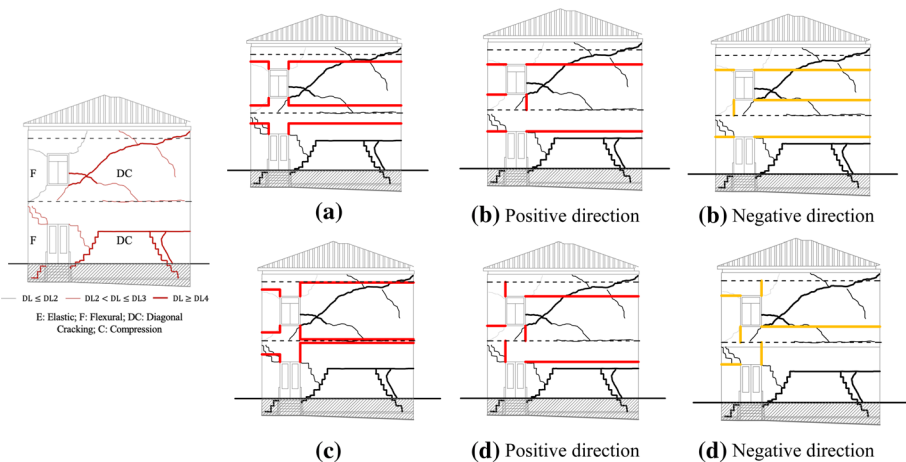


Fig. 3 Damage survey and wall equivalent frame idealization of W10: **a** Lagomarsino et al. (2013); **b** Augenti (2006); **c** Dolce (1991); **d** Moon et al. (2006)

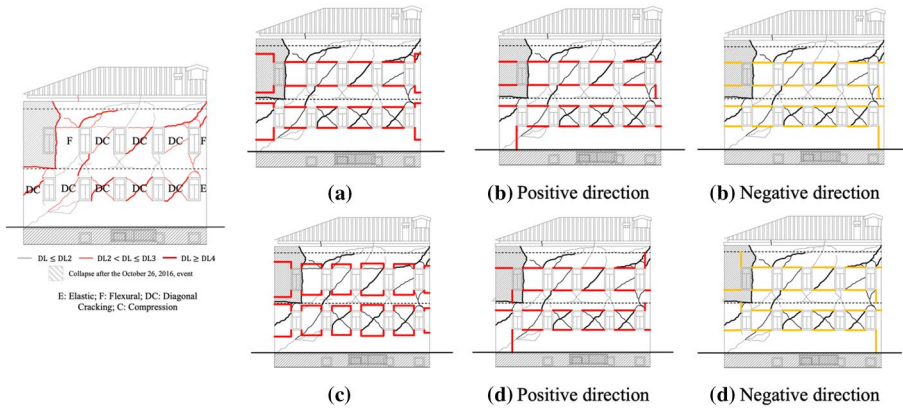


Fig. 4 Damage survey and wall equivalent frame idealization of W8: **a** Lagomarsino et al. (2013); **b** Argenti (2006); **c** Dolce (1991); **d** Moon et al. (2006)

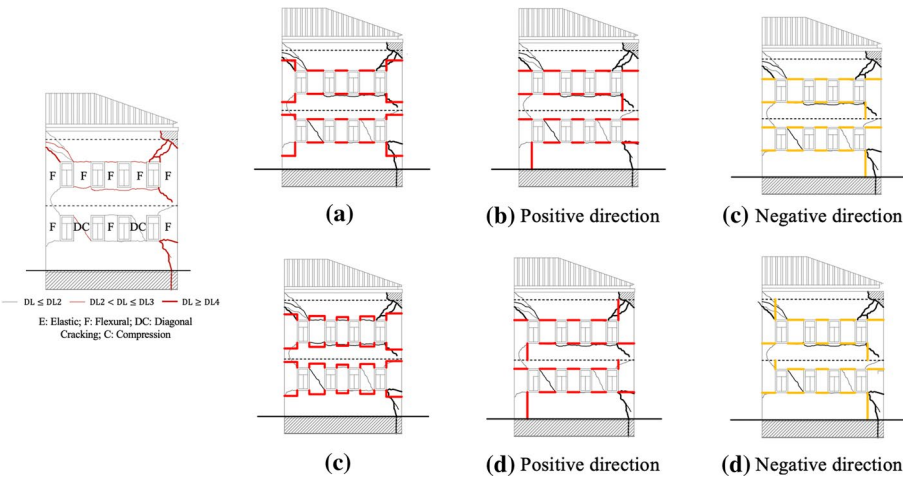


Fig. 5 Damage survey and wall equivalent frame idealization of W6: **a** Lagomarsino et al. (2013); **b** Argenti (2006); **c** Dolce (1991); **d** Moon et al. (2006)

direction) is overlapped to the actual damage survey (in black); the dashed lines define the average floor height. The represented façades refer to the actual configuration of the structure. Yet, it is worthy observing that for the purposes of the research activity of the “*URM nonlinear modelling—Benchmark project*” some simplifications in the considered structural configuration have been made, including that of neglecting the explicit modeling of both the basement floor (in grey in Figs. 3, 4 and 5), which involved only a minor part of the floor plan, and the roof. The ground level conventionally adopted in the modelling of the structure is represented in these Figures through a horizontal black line.

As it clearly results, the main difference between the four criteria is found in the external piers, whereas in almost all the cases, the inner elements are characterized by effective heights that follow the aligned openings; only for the criterion by Dolce (1991) the resulting height for the internal piers is a bit higher. The comparison with

the actual damage of these elements shows how the cracks (both in the case of diagonal cracking and of flexural failure) spread typically in a height equal to that of the adjacent openings. In the case of the external piers, the criteria proposed by Moon et al. (2006) and Augenti (2006), which are mostly based on considerations related to the development of an equivalent strut in the considered direction of analysis, seem to alternatively well capture the cracks at the upper or lower end of the elements. The adoption of such criteria requires alternative models for monotonous analysis in X and Y directions, with a significant increase in the computational effort. The criteria proposed by Lagomarsino et al. (2013) and Dolce (1991) appear therefore a reasonable compromise which, however, allow a very good match with the actual damage, considering also the cyclical nature of the seismic action and the simplification intrinsically made by EF models of neglecting the nonlinearity of node regions. Between these two criteria, that of Lagomarsino et al. (2013) finds greater agreement for external piers and this is the reason why the analyses discussed in Sect. 3 adopt this choice in a unified way across the SWs. Moreover, in Sects. 4.3 and 5.2 the effects resulting from the adoption of alternative criteria are discussed in terms of pushover curves and safety verification.

Regarding the spandrels, in the literature the alternative proposals are very limited (Lagomarsino et al. 2013). In the case of regular pattern of the openings, that corresponds also to the configuration of the “P. Capuzi” school, the criterion commonly adopted is to assume the size of the spandrels equal to the masonry portion between the vertically aligned openings. This rule is confirmed by the observation of the damage occurred in the school and is the one adopted in all the analyses discussed in the following sections. Of course, more critical and debated is the case of not aligned openings which some recent literature works are addressed to (e.g. Parisi and Augenti 2013, Berti et al. 2017, Siano et al. 2018) but that is out of the scope of paper and not representative of the BS under examination. Finally, Figs. 3, 4 and 5 also introduce some useful data for checking the reliability of the SWs, at least in a qualitative way, in terms of comparison with the damage pattern (as later discussed in Sect. 3.4).

To make more direct and effective such a comparison:

- First of all, the damage level (DL_E) attained in each panel has been attributed, roughly classified as: $DL_E \leq DL_{E2}$ corresponding to hairline or slight cracks; $DL_{E2} < DL_E \leq DL_{E3}$ corresponding to large and extensive cracks; $DL_E \geq DL_{E4}$ corresponding to a serious failure, close to the complete loss of sustaining horizontal loads and possibly even the vertical ones.
- Then, tags consistent with those adopted in Sect. 3.4 to anonymously illustrate the damage pattern simulated by the software have been added over each panel. In particular, the main failure mode activated in the panel has been identified as *F-flexural* or *DC-diagonal cracking*. When no visible cracks were observed the tag *E-elastic* has been assigned; of course, that is a bit conventional, since the full “elastic phase” is purely ideal in a building so severely damaged. Concerning the attribution of the tags “F” and “DC”, it is evident that in some cases a mixed mode occurred, that is characterized by cracks associated to both a partialization of the end sections and diagonal cracks: in those cases, the damage mode has been associated on the basis of the highest gravity of the cracks. This choice – although conventional—was made to make clearer and easier the damage interpretation.

3 Sensitivity of results to different software packages with standardized modelling assumptions

This section describes the results of the analysis carried out on BS5 through the SWs set as much as possible under similar modeling hypotheses, as introduced in Sect. 2.

The following parameters, obtained from the performed analyses, are here compared:

- The total mass of the building.
- The periods, participant masses and modal shapes obtained from the modal analysis (Sect. 3.1).
- The global pushover curves (Sect. 3.2) and the synthetic parameters that univocally define the equivalent bilinear curves (i.e. the stiffness K_s , the base shear V_y and the ultimate displacement d_u) (Sect. 3.3).
- The damage pattern (Sect. 3.4). Only for the case BS5/C, the damage corresponding to the ultimate displacement capacity (d_u) evaluated on the pushover curves has been also compared with the actual one occurred in the “P. Capuzi” school.

The conversion of the pushover curve into a bilinear equivalent curve is particularly useful: firstly, to more effectively quantify the dispersion on results; secondly, because it represents a functional step in order to apply most of nonlinear static procedures adopted in the literature (e.g. the N2 Method originally proposed in Fajfar 2000) and in the Codes [e.g. in EC8-3 (CEN 2005); NTC 2018; ASCE 41–13 (2017)]. The second aim allows thus to make a comparison also on parameters that have a direct impact on the seismic safety assessment.

3.1 Comparison of masses and dynamic parameters estimated by the modal analysis

Table 2 summarizes the total mass estimated by the six SWs and the percentage variation with respect to the reference value obtained from the hand calculation. In the legend of Table 2 the contributions associated to the gravity loads transmitted by the floors, those of the load-bearing walls, those of the r.c. tie beams, etc. are also distinguished in order to more easily identify potential discrepancies between the reference value and the estimate obtained by the SWs, if any. In the Table, the item “attic masonry” refers to the contribution offered by the portions of masonry pertaining to the attic on which the roofing elements lie on; this is consistent with the simplification of modelling the roof just as an equivalent mass. This preliminary comparison allows to avoid gross errors deriving from inconsistent input data insertion: in all cases the percentage variation is lower than 5% (in most cases even significantly lower).

In the following, the comparison of the dynamic parameters estimated by the SWs through the execution of the modal analysis is presented. Conventionally, the modal analysis was carried out by adopting the cracked stiffness values (i.e. the same values then adopted in the non-linear static analyses).

In particular, the first three modes are analyzed in terms of periods, participating masses and modal shapes. The comparison is made referring “to the same vibration mode”, that is having selected for each SW the consistent modes through an equivalence criterion based on the comparison of the participating masses. To this aim, for all the SWs the results of up to the first ten vibration modes have been considered, checking that the significant

Table 2 Total masses estimated by the SWs and reference value obtained by the hand calculation

	BS5/A		BS5/C	
	M (kg)	ΔM % (on manual estimation)	M (kg)	ΔM % (on manual estimation)
SW1	3,120,517	−3	3,247,237	−3
SW2	3,128,517	−3	3,253,787	−2
SW3	3,176,934	−1	3,305,086	−1
SW5	3,283,790	2	3,418,101	2
SW6	3,227,043	0	3,337,450	0
SW7	3,338,109	4	3,313,014	−1
Hand calculation ^a	3,220,831	−	3,336,031	−

^aThe weight of the various contributions on the total mass results as follows: masonry wall (69% for BS5/A and 67% for BS5/C); dead load of intermediate diaphragms (12%); dead load of roof (3%); accidental loads (3%); additional load on the top wall due to attic masonry not explicitly modelled (13% for BS5/A and 12% for BS5/C); r.c. tie beams, only for BS5/C (3%)

modes for such a comparison (i.e. those characterized by the highest participating mass) were within the first three. This assumption is justified by the fact that the BS is characterized by rigid floors, able to couple the walls in a significant way.

Table 3 summarizes for each SW the modal participating masses in the X and Y directions (as illustrated in Fig. 1) of the selected modes. Instead, Table 4 illustrates the identification of the selected reference modes for both the considered cases (BS5/A and BS5/C); it also reports the reference values $T_{i,av}$ of the periods obtained for each of the three considered modes, evaluated as the average of the values obtained by the six SWs.

The results of the modal analysis show in most cases a flexural–torsional vibration mode (named as “X–Y”), characterized by percentages of activated participating mass along both the X and the Y directions, and two more translational modes (named as “X” and “Y”, respectively). Of course, these definitions have to be considered “conventional” since, due to the in-plan irregularity, “pure” (i.e. in the sense of “ideal”) torsional and translation modes were not detected. Considering all these three modes, the participating mass activated is equal to or greater than 80% in both directions. Moreover, from the $T_{i,av}$ values in Table 4, it may be observed that the periods of the “Y” and “X–Y” modes are quite close in this structure, while the periods of the two translational modes “X” and “Y” are more distinct.

The two SWs that exhibited the highest differences are SW6 and SW7, as it results from Table 3. However, in the case of SW6, it has to be observed from Table 4 that the type of the first two predicted modes (“X–Y” and “Y”) is reversed with respect to the other SWs. As afore mentioned, the periods of the first two modes are very close one to each other; thus, it appears reasonable that small differences in the distribution of masses and stiffness may justify this reversal. Having that in mind, the differences in the participant masses are not so huge when compared to the other SWs. Conversely, the different behavior obtained by SW7 is much more appreciable. In fact, SW7 exhibits two almost purely flexural modes and a purely torsional third mode. This may be ascribed to the different way adopted in this SW to simulate the flange effect. This issue will be more in depth investigated in Sect. 4.1.

Table 3 Comparison of the participating masses obtained from different software

	First mode			Second mode			Third mode				
	Mx (%)		My (%)	Mx (%)		My (%)	Mx (%)		My (%)		
	BS5/A	BS5/C	BS5/A	BS5/A	BS5/C	BS5/A	BS5/C	BS5/A	BS5/C		
SW1	12	13	26	2	1	60	65	74	74	1	1
SW2	24	20	24	6	8	65	62	60	62	0	0
SW3	23	24	42	18	15	45	49	48	51	0	0
SW5	23	22	30	11	9	50	53	48	51	0	0
SW6	7	6	63	12	12	26	23	72	72	0	0
SW7	0	0	87	86	86	0	0	2	2	0	0

Table 4 Identification of the three main modes of the structure among those evaluated by the SW based on the comparison of the participating masses

SW	Modes		
	X–Y mode	Y mode	X mode
SW1	Mode 1	Mode 2	Mode 3
SW2	Mode 1	Mode 2	Mode 3
SW3	Mode 1	Mode 2	Mode 3
SW5	Mode 1	Mode 2	Mode 3
SW6	Mode 2	Mode 1	Mode 3
SW7	–	Mode 1	Mode 2
$T_{i,av}$ (BS5/A) (s)	0.246	0.249	0.226
$T_{i,av}$ (BS5/C) (s)	0.251	0.245	0.226

– Not identified mode

Figure 6 illustrates the percentage variation of the periods calculated by the six SWs with respect to the reference values of BS5/C, together with the modal shape of the three reference modes selected by the SWs according to Table 4. It emerges that, for all the SWs, the differences are lower than 5% and, in most cases, even lower than 2.5%. Moreover, the components of the eigenvectors have been obtained only for some few points of the structure, in order to reconstruct, even if in a simplified way, a plan-view of the modal shapes. As expected in a linear analysis, there are no significant differences in terms of modal shapes (neither in terms of periods) passing from cases BS5/A to BS5/C (being the coupling offered to piers by the spandrels exactly the same and independent from the strength properties). For this reason, Fig. 6 reports only the modal shapes with reference to the case BS5/C, assuming the modes listed in Table 4.

3.2 Comparison in terms of global pushover curves

Nonlinear static analyses were carried out in the two main directions of the structure (X and Y), neglecting the effect of any additional eccentricity and considering both positive and negative directions of the seismic action. In addition, two different load patterns were applied, respectively proportional to the mass distribution (named "uniform" in the following) and to the product of the masses and the height of the structural nodes (named "inverse triangular", and synthetically called "triangular" in the Figures). Although the irregular plan of the building would suggest further interesting investigations on the use of other horizontal load patterns or more refined nonlinear static procedures, able to better account for the higher and torsional modes (e.g. as discussed in Azizi-Bondarabadi et al. 2019 or Aşıkoğlu et al. 2021), these issues were out of the scopes of the research activity, mainly focused on comparing the results provided by EF models when adopted by using the same modelling and analysis method assumptions. Thus, also in performing the nonlinear static analyses and representing the results, the RTs adopted common hypotheses on the load pattern, the displacement plotted in the pushover curves and the choice of the control node (as much as possible close to the centre of masses).

A total of eight different analyses were considered for each case (BS5/A and BS5/C). Figure 7 shows the obtained pushover curves for both the load patterns and, by way of example, for the positive direction of analysis.

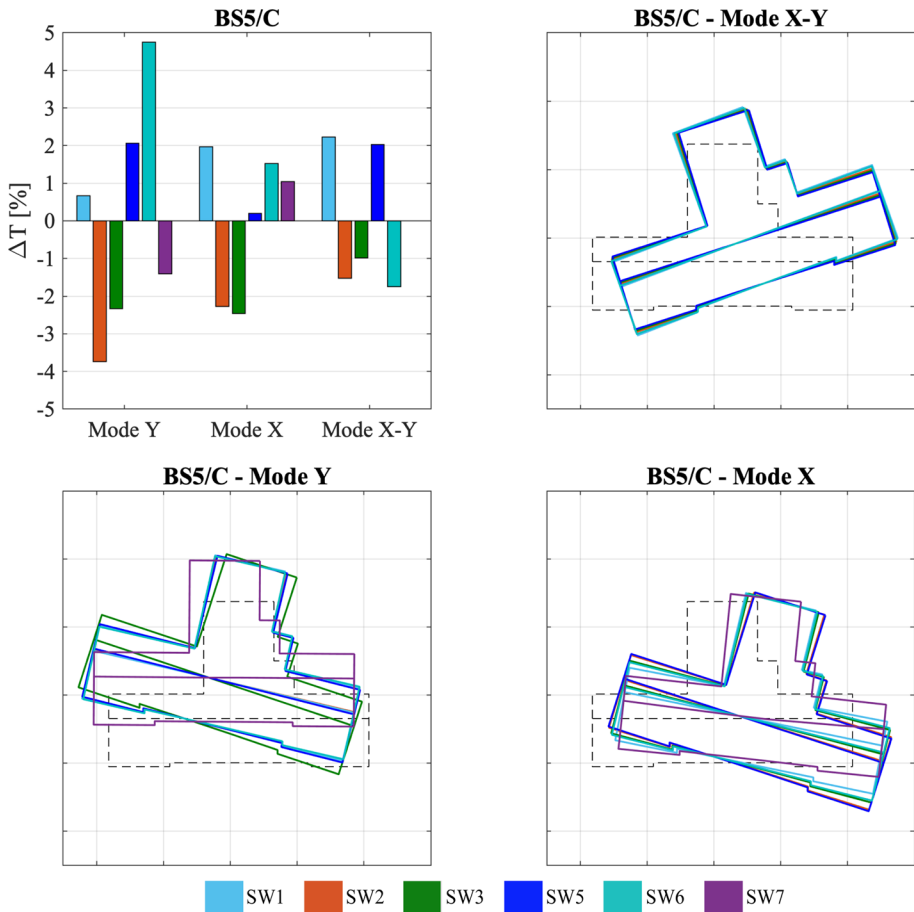


Fig. 6 Percentage variation from the reference value of modes in X, Y and X–Y and Modal shapes and undeformed configuration (the dashed black line) for the first floor: Case BS5/C

Passing from case BS5/A to BS5/C, a trend similar to that observed in other benchmark structures (e.g. Manzini et al. 2021 for BS4 and Degli Abbati et al. 2021 for BS6, respectively) can be observed, characterized by an increase of the initial stiffness and of the overall base shear and a reduction of the ultimate displacement capacity.

3.3 Percentage variation of the three parameters defining the equivalent bilinear curves

The pushover curves reported in Sect. 3.2 have been converted into equivalent bilinear curves. Table 5 shows the average and dispersion values conventionally adopted as reference for the comparisons discussed in the following; they refer to the three parameters that describe the bilinear curves (namely V_y , K_s and d_u as introduced in Sect. 3).

Figure 8 shows the percentage variation of the results obtained by the SWs with respect to the reference (i.e. “average”) values of Table 5. It can be observed that:

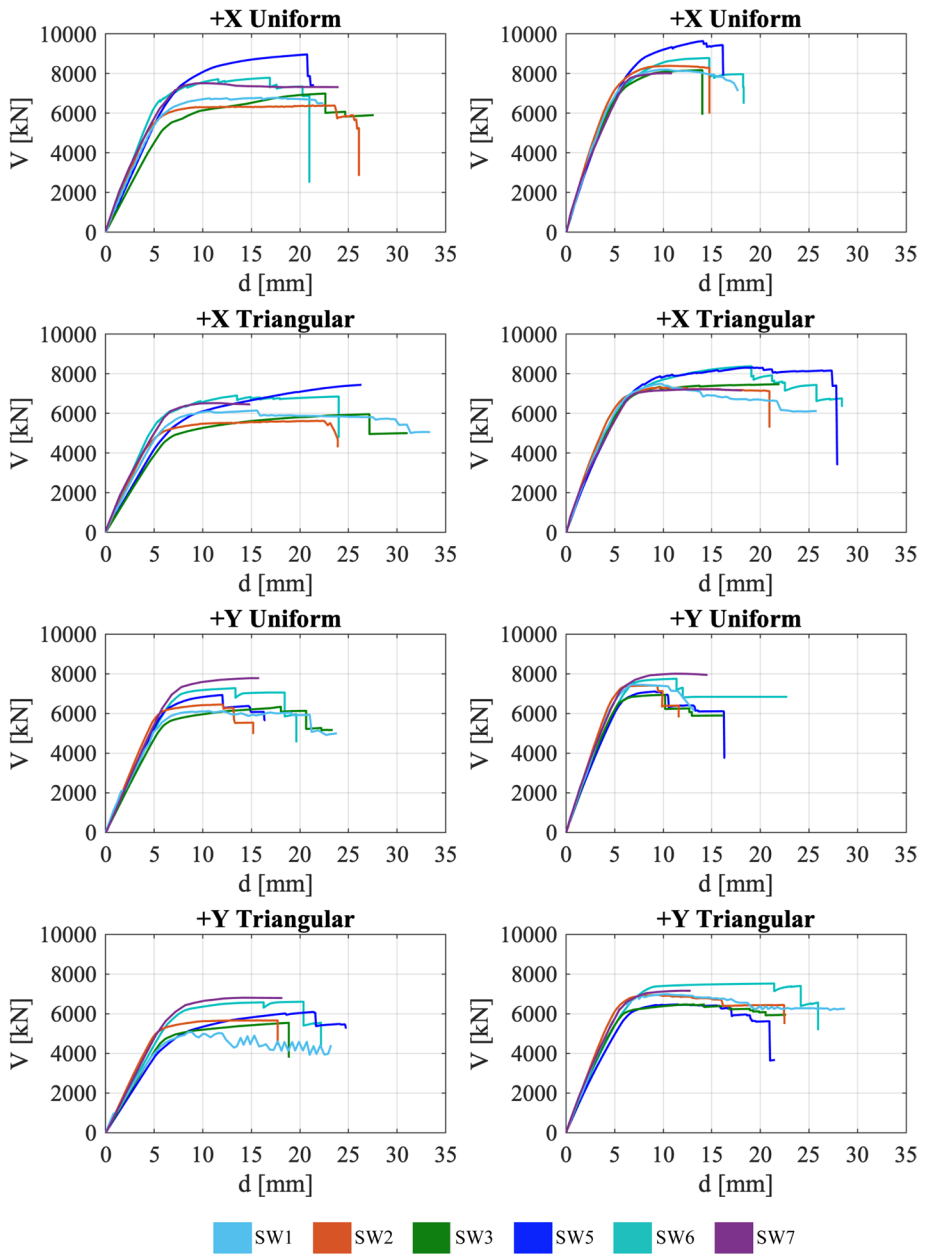


Fig. 7 Comparison of the global pushovers obtained for Case BS5/A and BS5/C for both directions and load patterns

- Stiffness (K_y): the percentage variation with respect to the reference value is limited to a maximum of 22% and 11%, respectively, for BS5/A and BS5/C.
- Overall base shear (V_y): the percentage variation is limited to a maximum of 19% and 11% for BS5/A and BS5/C, respectively.

Table 5 Average and dispersion of the three parameters defining the equivalent bilinear curves obtained for both directions and load patterns (U stands for “uniform” and T for “inverse triangular”); cases BS5/A and BS5/C

Analysis	V_y (kN)		K_s (kN/mm)				d_u (mm)					
	BS5/A		BS5/C		BS5/A		BS5/C		BS5/A		BS5/C	
	μ	σ	μ	σ	μ	σ	μ	σ	μ	σ	μ	σ
X+U	7076	0.11	8241	0.06	1139	0.13	1452	0.05	24	0.13	15	0.19
X+T	6101	0.09	7366	0.06	945	0.18	1224	0.06	26	0.15	24	0.18
X-U	7711	0.08	8526	0.06	1087	0.14	1401	0.06	21	0.13	18	0.19
X-T	6757	0.07	7871	0.06	901	0.14	1173	0.06	28	0.20	24	0.11
Y+U	6490	0.10	7031	0.07	1058	0.07	1364	0.07	19	0.20	16	0.23
Y+T	5654	0.13	6663	0.06	877	0.11	1159	0.08	21	0.14	22	0.28
Y-U	6936	0.03	7345	0.06	1075	0.09	1361	0.07	18	0.19	16	0.27
Y-T	6220	0.08	7226	0.08	894	0.12	1150	0.08	22	0.09	21	0.25

K_s has been defined imposing the passage for the value of the base shear equal to 0.7 of the maximum overall base shear reached; d_u has been defined stopping the curve at the base shear decay of 20%; V_y has been derived by applying the equal area rule based on energetic principles

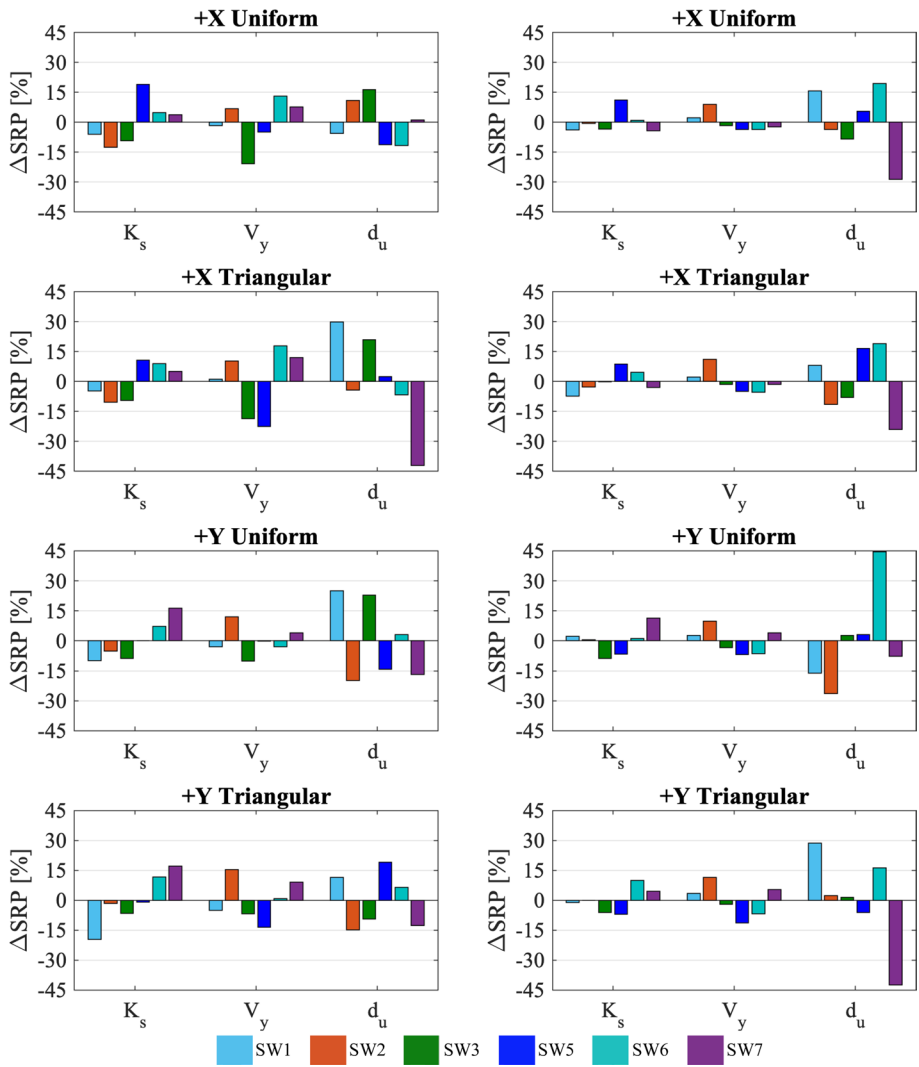


Fig. 8 Percentage variations of the three parameters that define the bilinear curves for both directions and distributions: cases BS5/A and BS5/C

- Ultimate displacement (d_u): the percentage variation reaches a maximum of 42% for BS5/A and BS5/C.

Considering the obtained results, also compared with what emerged from the results of BS4 in Manzini et al. (2021) and BS6 in Degli Abbati et al. (2021), it can be observed that:

- The reduction of the percentage variation in the transition from case BS5/A to BS5/C is less appreciable in this structure, much more complex than BS4 (2-storey single unit URM building) and more irregular in the plan configuration than BS6 (complex URM

building inspired to the Pizzoli's town hall, characterized by an elongated rectangular shape).

- A greater variation of the ultimate displacement, with respect to the other considered parameters, is confirmed.

This latter result is imputable to a lower standardization of the drift calculation criteria adopted by the SWs, despite the fact that in all the SWs the same ultimate drift thresholds at element scale have been adopted (see Sect. 2). In fact, as discussed in Cattari and Magenes (2021) and Cattari et al. (2021a), different approaches are usually adopted for the drift computation in the SWs, such as: the simple ratio between the difference between the horizontal displacements at the end sections and the panel effective height; the chord rotation; its equivalence with the plastic component of the rotation. This is a consequence of the fact that most seismic Codes recommend thresholds for the “drift” to check the attainment of the collapse at element scale without clarifying the criteria to compute it. Since these criteria are autonomously defined by the software package without usually giving the possibility to users to change them, it results in a potentially high scatter of the ultimate displacement capacity on pushover curves.

3.4 Comparison of the damage failure modes predicted by the software packages at the ultimate displacement

The results shown below refer to the analysis step corresponding to the achievement of the ultimate displacement (d_u), as obtained from the nonlinear static analyses performed with the different SWs considering the “uniform” load pattern, both the X and the Y directions and the positive direction of the lateral forces. The data on the damage (failure mode and severity) has been post-processed for each structural element, according to the general criteria adopted in the “*URM nonlinear modelling—Benchmark project*” and introduced in Cattari and Magenes (2021). In particular, two types of comparison have been adopted: one able to exhaustively show the damage localization in each element and to interpret the global failure mode activated at the scale of each wall; another addressed to provide in an aggregate way a synthetic overview of the consistency on the simulated damage across the SWs. This second type of damage representation (Figs. 9, 10, 11, 13 and 15) reports, for each element, the number of SWs that predicted the same failure mode; thus, obviously, in the case of perfect agreement among the SWs, the number in the ordinate axis exactly corresponds to that of the software package. In both cases, an anonymous format of comparison has been adopted. For sake of brevity, the attention is mainly focused on the results related to the perimeter walls; moreover, depending on the direction of analysis, only the walls more involved in equilibrating the seismic actions and more affected by the damage (unless significant torsional phenomena) have been selected. The numbering of the walls refers to Fig. 1; the complete numbering of the structural elements is listed in the Annex I made by Cattari and Magenes (2021).

In general, the comparisons show a good agreement among the predictions obtained by the different SWs, as well as between the numerical results and the actual response of the building (see also Fig. 3, 4 and 5); obviously the latter consideration only concerns to BS5/C, which is the case more consistent with the actual building configuration.

First of all, the consistency on the damage failure modes predicted by the SWs is discussed.

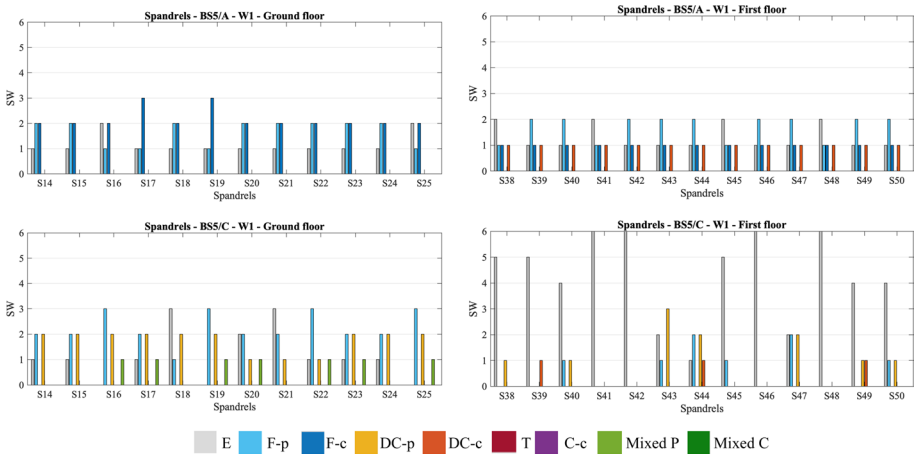


Fig. 9 Comparison of the damage predicted by software for the spandrels of Wall 1 at the Ground and First Floor BS5/A and BS5/C: +X analysis

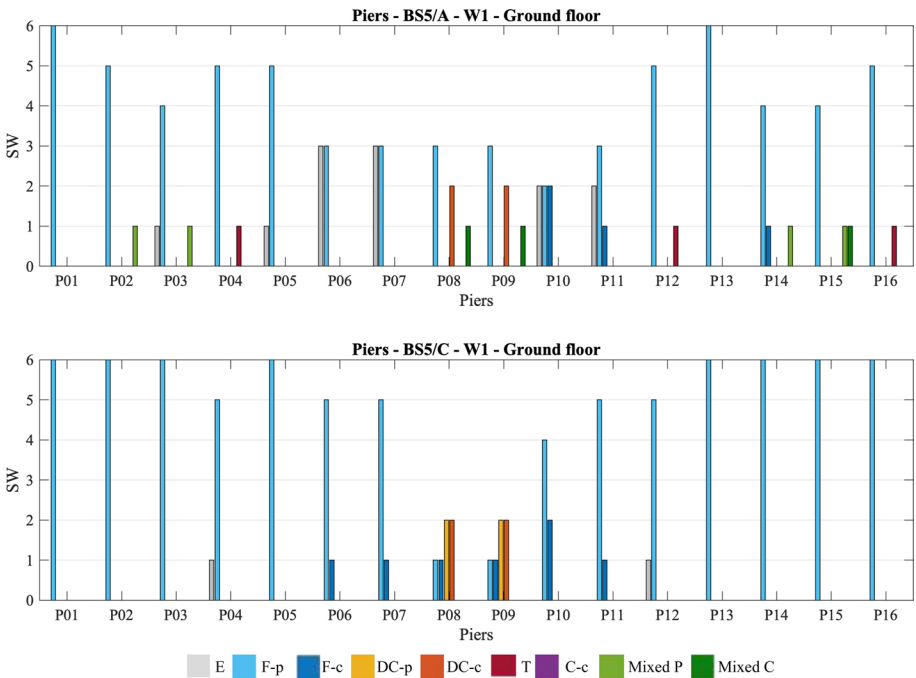


Fig. 10 Comparison of the damage predicted by software for the piers of Wall 1 at the Ground Floor BS5/A and BS5/C: +X analysis

The considered damage states of the structural elements, reported in the caption of the following Figures, are: E: Elastic; F-p: Flexural-plastic; F-c: Flexural-collapse; DC-p: Diagonal Cracking-plastic; DC-c: Diagonal Cracking-collapse; T: Tension; C-c: Compression-collapse; Mixed P: Mixed Plasticity; Mixed C: Mixed Compression.

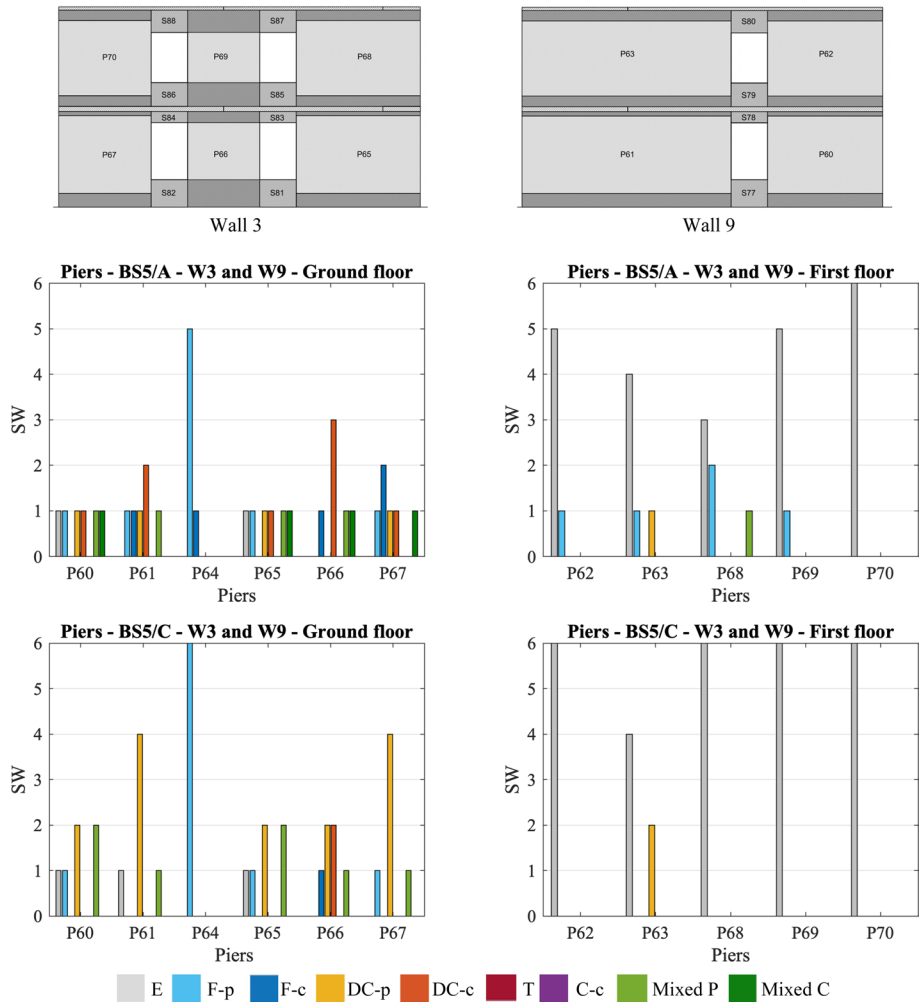


Fig. 11 Comparison of the damage predicted by software for the spandrels and piers of W3 and W9 at the ground floor BS5/A and BS5/C: +X analysis

Compression-collapse; Mixed-p: Mixed shear and flexural-plastic; Mixed-c: Mixed shear and flexural-collapse.

With reference to the X-direction of analysis, it is observed that:

- Spandrels.* Starting from wall W1 (Fig. 9), almost all of the SWs estimate the flexural plasticization (or collapse) in case BS5/A (“weak spandrel” behavior), whereas, moving to case BS5/C, more differentiated failure modes can be observed, even if the most recurring one is the diagonal cracking shear failure mode (justified by the presence of the coupled r.c. tie beams). This trend has also been found for walls W3, W7 and W9. Figure 12 reports, by way of example, the extended damage pattern representation for wall W8, oriented in Y direction and discussed hereinafter. The passage from a prevailing flexural damage in case BS5/A to the diagonal cracking in case BS5/C is consistent

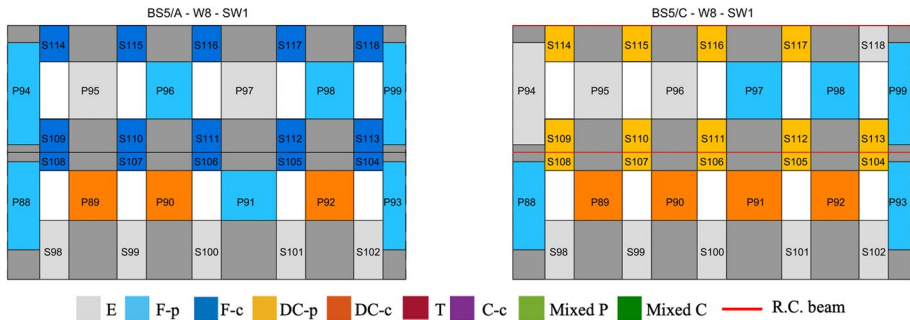


Fig. 12 Comparison of the damage predicted by SW1 for the spandrels and piers of W8: BS5/A and BS5/C, + Y analysis

with the strength criteria adopted for the interpretation of the response of the spandrel elements, which rely on the activation of the strut mechanism only in the case of the presence of a coupled tensile resistant element, a condition guaranteed in case BS5/C by the presence of the r.c. tie beams.

- Piers.** Starting again from wall W1 (Fig. 9), almost all of the SWs estimate a prevailing flexural damage in case BS5/A, more localized in the piers at the ground floor (indeed, most SWs predict an elastic response for the piers at the first floor). For some inner piers (i.e. P08 and P09, see Fig. 9 for the elements numbering), in case of BS5/C, the majority of the SWs predict a prevailing diagonal shear cracking, while only two SWs predict a flexural response. This discrepancy can be ascribable to the range of the axial load acting on the panels, which corresponds to the region of the strength domains in which the predictions of two failure modes are very close. Thus, small differences in the variation of the axial load on the elements can lead to differences in the failure mode predicted, as also discussed in detail in Manzini et al. (2021). Apart from this aspect, also in case BS5/C an overall consistency among the SWs in predicting the concentration of the damage at the ground floor can be observed. As regards walls W3 and W9 (Fig. 11), case BS5/A shows more scattered predictions, with a clear tendency, in the transition to BS5/C, to pass to a prevalence of diagonal cracking shear failure of the piers at the ground floor. The fact that the trend in this transition from BS5/A to BS5/C is less marked for wall W1 is justified by the geometry of the piers of this particular wall, which are much slenderer than those of the other ones, and for which (all other factors being equal) a greater propensity to a flexural failure is therefore reasonable.

With reference to the Y-direction of analysis, it is observed that:

- Spandrels.** Starting from walls W6 and W8 (characterized by a more significant number of spandrels and therefore more representative), almost all of the SWs estimate the flexure plasticization (or collapse) for case BS5/A, passing in most cases to the diagonal cracking shear failure mode or to the elastic phase in case BS5/C (Figs. 12, 13 and 14). The general behavior is therefore the same observed in the X direction.
- Piers.** Starting from W6 and W8 (Figs. 12, 13 and 14), in case BS5/A, almost all of the SWs estimate a prevailing flexural response of the elements, localized at the ground floor (most of the SWs predict an elastic response of the piers at the first floor). In case BS5/C, most of the SWs estimate a shear behavior concentrated at the ground floor,

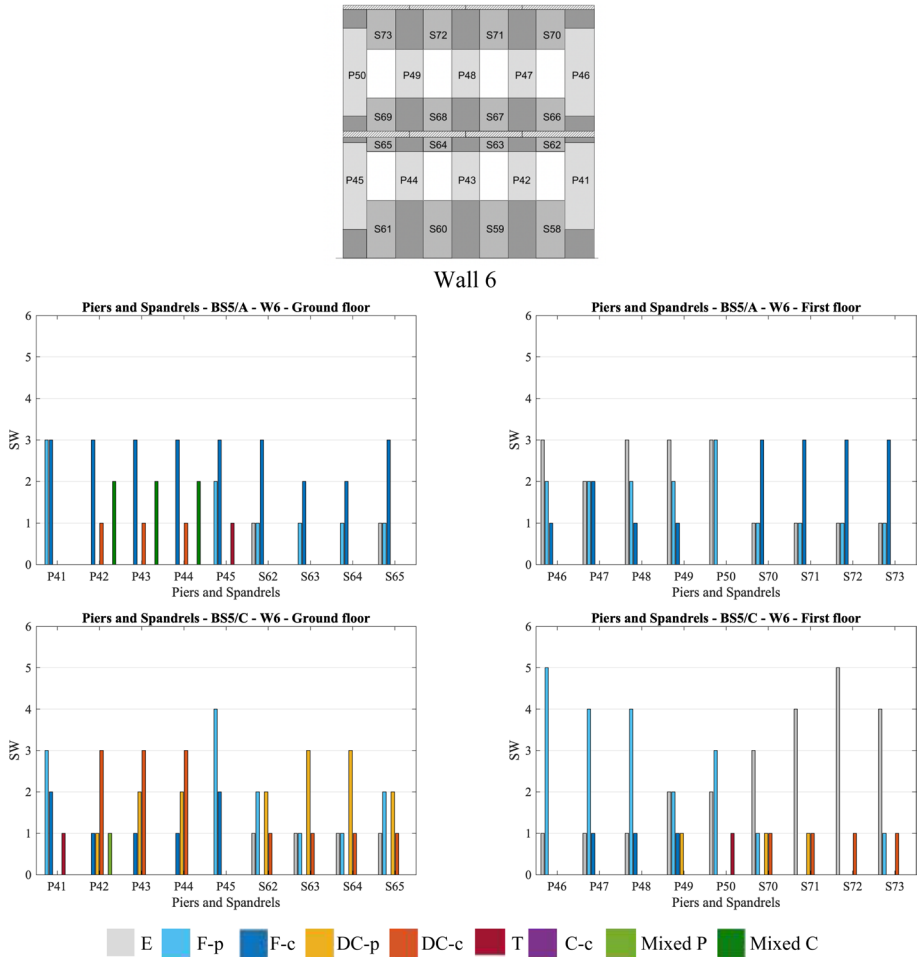


Fig. 13 Comparison of damage predicted by software for the spandrels and piers of W6 for the BS5/A and BS5/C + Y analysis

predicting for the piers of the first floor a still elastic behavior or a flexural plasticization. The same applies also for W10, as depicted in Fig. 15.

Finally, in the following some preliminary considerations are discussed on the reliability of the damage predicted by the SWs in case BS5/C against the structural response actually exhibited by the building inspiring the BS (see also Figs. 3, 4 and 5).

It is worth recalling that the school has been closed following the event of August 24, 2016, after which the building had already shown widespread damage in several walls. The structure subsequently suffered considerable and progressive worsening of the damage, that in the second shock of October 26, 2016 also led to the collapse of a portion of the external façade W7 (see Fig. 1). Overall, the damage reached by the building following the October 30 event can be classified as incipient collapse, with extremely limited residual

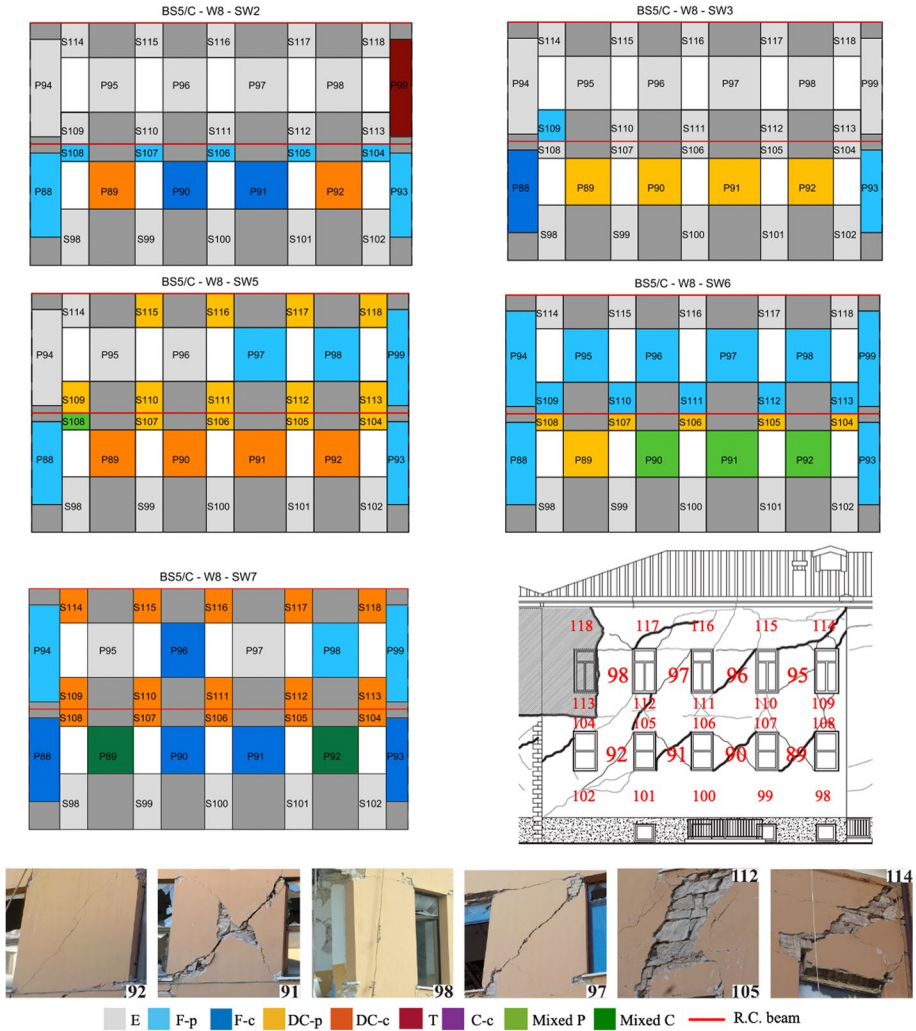


Fig. 14 Wall 8: comparison between the actual and simulated damage for the spandrels and piers (BS5/C: +Y analysis)

capacity to withstand horizontal actions. Considering the serious damage level suffered by the structure and the intensity of the seismic event (discussed in more detail in Brunelli et al. 2021), it appears reasonable to compare it with the damage predicted at the last step of the pushover analyses.

It is obvious that the analyses performed have not the ambition to accurately simulate the actual seismic response of this structure; thus, the comparison can be made only in qualitative terms. Moreover, it has to be highlighted that the severity of the actual damage in specific elements is also the result of damage accumulation phenomena, due to the complex seismic sequence that affected the area of the school, which the nonlinear monotonic static analyses presented in this document cannot describe. Nevertheless, the comparison is useful to check whether the damage pattern foreseen by the SWs is consistent or not with

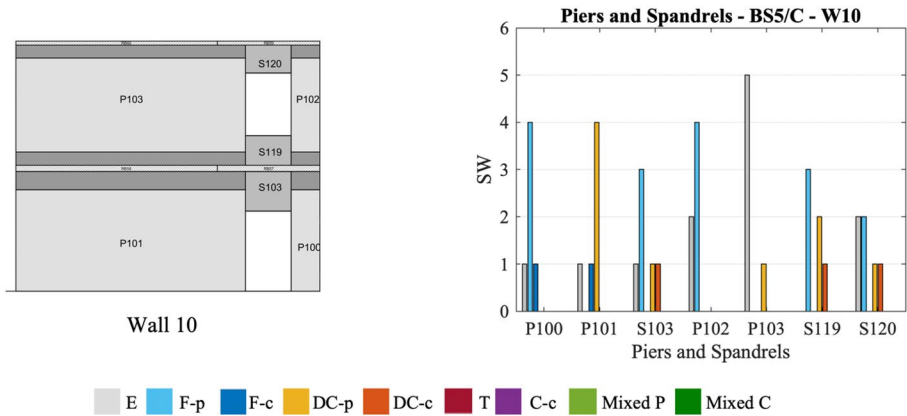


Fig. 15 Comparison of damage predicted by software for the spandrels and piers of W10 (BS5/C, + Y analysis)

the one actually occurred; in fact, the overall global failure mode occurred can be considered not altered by the phenomena of damage accumulation.

In general, a good agreement can be observed (see respectively Figs. 4 and 14 for W8, Figs. 3 and 15 for W10 and Figs. 5 and 13 for W6). In fact, as previously highlighted, in case BS5/C the SWs predict for the piers an overall response in general characterized by a more severe concentration of damage at the ground floor, with a prevalence of the diagonal cracking shear damage and with the flexural response limited to some elements at the first floor, whereas for the spandrels a shear response due to diagonal cracking or an elastic condition are predicted.

More precisely, Fig. 14 shows the detailed comparison between the simulated and the actual damage for wall W8 (for the results of SW1 please refer to Fig. 12). The numerical results refer to the analysis carried out in Y direction on the BS5/C configuration. Some pictures of the actual damage occurred in some piers and spandrels (dated to December 8, 2016) are included, too. In agreement with the actual response, it emerges that:

- The piers of the ground floor are more damaged than those of the first floor (having reached in most cases the collapse condition (C), i.e. the exceeding of the drift limit).
- The piers of the ground floor are affected by a prevailing diagonal cracking shear failure mode.
- The over-window spandrels of the ground floor are affected by a prevailing shear response (having in most cases reached only the plasticization condition, therefore a lower level of damage compared to the piers).
- The under-window spandrels of the first floor are affected by a lower level of damage than those on the ground floor.

In addition, according to the aggregate damage format, Figs. 13 and 15 allow to confirm the good match of results for W6 and W10, respectively; for the actual damage, please refer to Figs. 5 and 3. In particular:

- Concerning W6, the SWs are almost unanimous in predicting a diagonal cracking failure mode for the internal piers at the ground floor and a prevailing flexural damage

mode for all the other piers. In the case of spandrels, the SWs estimate an almost elastic response at the top level, in agreement with the elements not damaged in reality, while they overestimated the damage of the spandrels at the intermediate level.

- Concerning W10, first of all it is useful highlighting that it is characterized at each floor level by a very squat pier (responsible for balancing most of the external seismic forces) coupled to a very slender one. In most cases (4 over 6) the SWs predicted a diagonal cracking shear failure mode for the squat element, while they are unanimous in estimating a flexural failure mode for the slender one. Moreover, further in agreement with the actual damage, a concentration of the damage at the ground floor is observed.

4 Sensitivity to different modelling assumptions on the global response

4.1 Effectiveness of the wall-to-wall connection

This section aims to highlight the sensitivity of the seismic response evaluated by the EF models to alternative assumptions on the effectiveness of the coupling among incident walls (such as cantonal or T-intersection at the internal walls). When the coupling is perfect, as assumed in the results discussed in Sect. 3, the so-called "flange effect" (in the following synthetically named as FE) is achieved. The FE consists in the possibility of axial loads redistribution between the incident piers and in the stiffness increase of a pier lying in one direction due to the contribution of the connected pier lying in the orthogonal direction. In other words, the wall panels, assumed to have a rectangular section in the wall plane for the computation of the shear strength, can work as a T or L flanged section. As described in Cattari et al. (2021a), the topic has not yet been exhaustively investigated in the literature; therefore, at the present state of the research, there are no universally recognized rules either on the definition of the collaborative width of the orthogonal piers or on the consequent interaction effects (if limited to an alteration of forces redistribution or also to that of gross area to be considered in the computation of shear strength).

The SWs adopted in the research implement different strategies to manage the wall-to-wall connections. As depicted in Fig. 16, the condition of perfect coupling among walls is managed by the SWs by means of: a perfect kinematic coupling between the vertical displacement of the piers (Fig. 16a); equivalent connection beams characterized by very high bending and axial stiffness (Fig. 16b) or rigid links (Fig. 16c). Conversely, the RT that used SW7 managed this assumption through a modification of the cross-section typology of each pier, that is considered "T" or "L" shaped instead of rectangular, taking into account the collaborative contribution of the incident element and appropriately defining the size of the flange (Fig. 16d). More specifically, in the SW7 model, in the case of perfect coupling the length of the flange of the cross-section of each pier element at the intersection between two walls is assumed up to a maximum of half of the length of the orthogonal element.

The additional parametric analyses carried out in order to simulate different degrees of the effectiveness of the connection of the walls have been performed, by way of example, with three of the SWs adopted in this research (i.e. SW1, SW2 and SW7). To this aim, in cases SW1 and SW2, the default solution adopted by the software packages to model the condition of perfect coupling has been converted in the one depicted in Fig. 16b introducing equivalent beam elements, whose stiffness was suitably calibrated, between the upper nodes of the pier elements constituting the flanged wall.

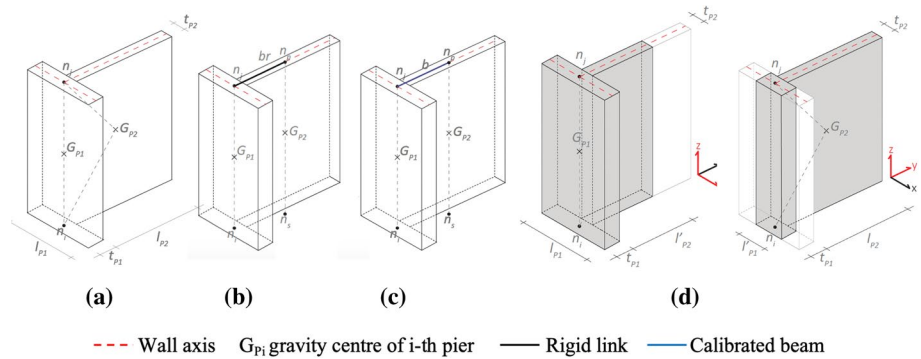


Fig. 16 Solutions adopted in SWs based on equivalent frame models for simulating the wall-to-wall connection: fully kinematic coupling by a degrees of freedom condensation (a) or a kinematic constraints (b); c use of equivalent calibrated beams; d definition of the collaborating flange (from Cattari and Magenes 2021)

The results obtained for BS5 and presented in the following cannot be assumed as exhaustive and general in absolutely quantitative terms. In fact, the coupling effect can be more or less significant due to the specific configuration of the walls of the building under examination. For instance, the presence of openings in proximity of the corner or of the internal wall intersection can significantly limit the role of the actual effectiveness of coupling, being limited by “geometrical” factors. In general, the effect is more pronounced in presence of squat panels intersecting. Actually, BS5 offers the occasion to discuss these issues by comparing the different results achieved in the X and in the Y directions, due to a different geometrical configuration of the structural scheme. Finally, it is worth noting that the flange effect and the contribution given by the out-of-plane flexural response of piers are not decoupled. Thus, a complete overview on the issue is provided by considering all the possible alternative on the two modelling hypotheses. In the following, the results of analyses carried out neglecting the contribution of the out-of-plane flexural response of piers, analogously to what assumed for the results discussed in Sect. 3, are presented. Then, additional comments on the combined effect of such aspects are discussed in Sect. 4.2.

4.1.1 Criteria adopted to simulate alternative modelling options on the wall-to-wall connection

The parametric analyses have been carried out considering:

- Two additional hypotheses on the effectiveness of the wall-to-wall connection, namely: an “intermediate” and an almost negligible (“poor”) degree of effectiveness (please note that the results presented in Sect. 3 refer to the case of full perfect coupling).
- Two alternative hypotheses on the quality of the connection between the walls oriented along the X and the Y directions: in particular, in one case the same hypothesis on the effectiveness of the wall-to-wall connection has been consistently adopted in the whole model, while in the other the quality of the connection has been altered only in some of the internal walls oriented in the Y direction (see Fig. 18a).

The calibration of the equivalent beams adopted to simulate different degrees of effectiveness of the wall-to-wall connection represents a quite tricky issue, since it would account for the geometry and properties of the incident piers and the masonry type (i.e. dimensions of block and bond type). However, in absence of an analytical formulation univocally recognized in literature, in this research such calibration is carried out reducing progressively of an order of magnitude the value of the moments of inertia J of the connecting beams and assuming such value equal for all the incident piers. The “starting reference value” for the stiffness of the equivalent beams (from which the reduction has been applied) has been calibrated in order to reproduce the same solution obtained in the case of perfect coupling (i.e. that corresponding to the solution obtained by the modelling option represented in Fig. 16a–b).

Table 6 summarizes the values assumed in the three SWs adopted to perform these parametric analyses varying the hypothesis on the quality of the connection. In the case of the “poor” connection it has been verified that a further reduction of the stiffness doesn’t change the results (i.e. the solution obtained actually correspond to the lower bound).

4.1.2 Results in terms of effects on the pushover curves

The following figures (Figs. 17 and 18) illustrate the results obtained with the three SWs used for the analyses in the limit conditions of perfect (continuous line) and poor (dashed line) coupling quality. The results refer to both the configurations, BS5/A (with “weak spandrels”) and BS5/C (with r.c. tie beams), when the same hypothesis is extended to the whole building. It is worth recalling that in the case of BS5/A the spandrels in SW7 have been directly modelled through axially rigid rods, without imposing any control on the ultimate drift. The results show a not-negligible sensitivity on all parameters characterizing the pushover curve: initial stiffness, yielding base shear and ultimate displacement capacity.

In the case of BS5/C, the differences in the response of the models, passing from the perfect to the poor connection, are also accompanied by changes, in some masonry panels, of the prevailing damage mode activated (in particular, from shear to flexural response); this aspect, evident from the different obtained pushover curves, is justified by the variation of the normal force distribution in the panels due to the different degree of coupling. The effects are more pronounced in the Y direction, although appreciable also in the X one; this is due to a different geometrical configuration of the piers in the two directions, as already discussed in Sect. 4.1.1.

The results show how the degree of effective connection between the incident walls represents an important epistemic uncertainty to be analyzed, in the knowledge phase of the structure, not only in relation to the vulnerability of the structure to the activation of possible local mechanisms but also for a more reliable evaluation of the in-plane global response. The sensitivity analysis adopted to calibrate the equivalent beams, which can be monitored through the variations of the results on the pushover curves and on the dynamic properties estimated by the modal analysis, is therefore effective to define a plausible range of variation of stiffness to be assigned to the beams and can be replicated for all structures under examination also to address the relevance of this epistemic uncertainty (and, as a consequence, also the plan of investigation techniques to be applied in the knowledge phase).

Table 6 Hypothesis assumed in the examples aimed to simulate the different degrees of connection

Quality of the connection	Solution implemented by the SW (according to Fig. 16)	d (altered stiffness of the pier)
Perfect	c (equivalent beam with calibrated stiffness)	
	Starting reference values: SW1 $A = 10 \text{ m}^2$, $J = 5 \text{ m}^4$, $EJ = 1.4e11 \text{ kNm}^2$ SW2 $A = 900 \text{ m}^2$, $J = 3.375 \text{ m}^4$, $EJ = 1e8 \text{ kNm}^2$	SW7—Extension of the wing equal to a maximum of the half of the length of the orthogonal wall
Intermediate	SW1 and SW2: Reduction of 2 orders of magnitude of the starting reference value	SW7- Flange extension equal to 4 times the thickness of the web in the case of the "L" section and 5 times the thickness of the web in the case of the "T" section
Poor	Reduction of 3 orders of magnitude of the starting reference value	SW7—No collaborating flange is considered; rectangular resistant pier section

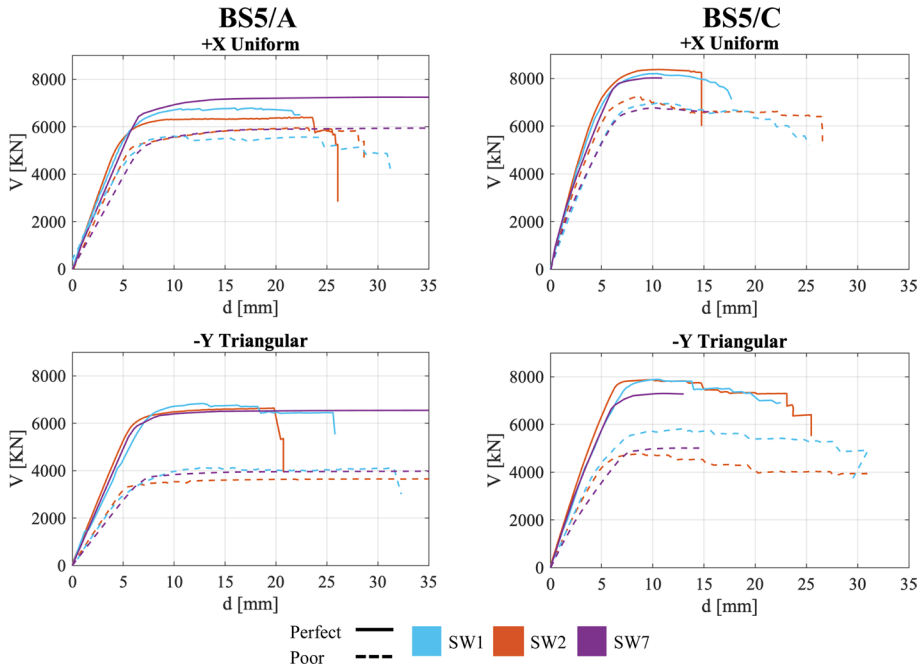


Fig. 17 Sensitivity of the pushover curve to the effectiveness of the wall-to-wall connection among incident walls in the BS5/A and BS5/C (same hypothesis adopted on the whole building)

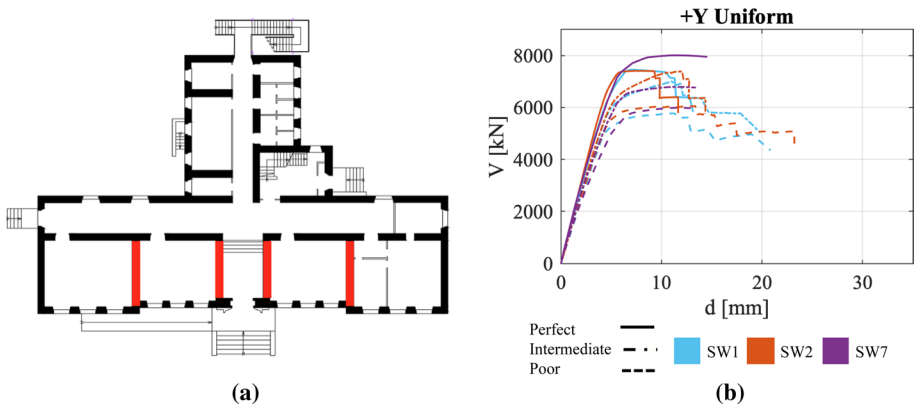


Fig. 18 a Identification of the piers oriented in Y direction for which the quality coupling among walls has been altered; **b** Sensitivity of the pushover curve to the effectiveness of the wall-to-wall connection among incident walls in case BS5/C—the coupling is altered only for piers marked in red in Fig. 18a

As an example, Fig. 18b illustrates the results obtained in the case in which the degree of coupling is altered (reduced) only in some of the internal piers oriented in Y the direction (as identified in Fig. 18a).

4.2 Contribution of the out-of-plane capacity of piers

The objective of this section is to study the contribution offered by the out-of-plane behavior of piers (OP in the following). The results reported below have been obtained using four SWs among those adopted (SW2, SW3, SW5 and SW6) that allow to consider in the analysis the flexural out-of-plane contribution of the panels both in terms of stiffness and strength. It is important to specify that the out-of-plane contribution still refers to the reper-cussion on the “global” in-plane response and should not be confused with the possible activation of “local” mechanisms.

4.2.1 Criteria adopted to simulate alternative modelling options on the out-of-plane piers contribution

In order to investigate the potential incidence on the overall base shear offered by the out-of-plane contribution of piers, the flexural strength domains associated to both the in-plane and the out-of-plane response of a masonry pier characterized by 2.50 m length, 0.40 m thickness and 2.50 m height are reported in Fig. 19a; in both cases, the calculation has been made by adopting the compressive strength of masonry reported in Table 1 for the cut stone.

Analogously to the in-plane flexural response, the bending out-of-plane contribution is computed according to the following expression:

$$M_{pl} = t^2 l \frac{\sigma_0}{2} \left(1 - \frac{\sigma_0}{\kappa f_m} \right) \tag{1}$$

where σ_0 is the mean vertical compressive stress acting on the full section and, under the hypothesis of an equivalent rectangular stress block of normal stresses of height κf_m , κ is the stress-block equivalence coefficient, assumed equal to 0.85. Figure 19b illustrates the strength domains of the pier varying the thickness t .

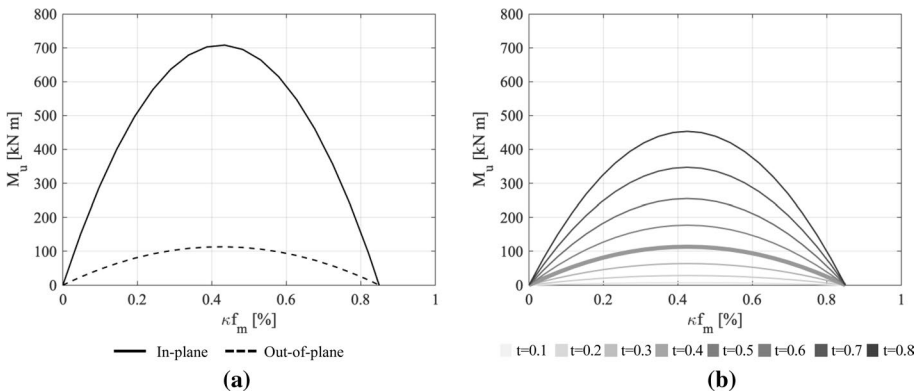


Fig. 19 a In-plane and out-of-plane flexural strength domains (assuming for the pier a thickness equal to 0.40 m); b Out-of-plane strength domain of the pier varying the thickness t , the values corresponding to a wall of 0.40 m has a thicker line

As far the possible interaction domain due to the bi-axial bending, most of software packages used (i.e. three of the four) consider in a simplified way the two domains as independent; only one software introduces a simplified interaction domain.

As it is obvious from Eq. (1), increasing the thickness the strength grows more than proportionally, being the bending moment proportional to the square of the thickness. However, it can be considered that, at least in traditional buildings, for wall thickness lower than 0.40 m (whose corresponding domain is represented with the thickest line in Fig. 19), the incidence of the out-of-plane contribution is not particularly significant and neglecting it is anyhow in favor of safety, whereas, for thickness greater than 0.40 m, this contribution becomes progressively more significant and neglecting it could lead to appreciable underestimations of the overall base shear of the building.

In the following section, the quantification of such a contribution on the pushover curves obtained for BS5 is illustrated; it is of interest recalling that in BS5 structural walls have thickness ranging from 0.53 m (longitudinal walls of the first floor) up to 0.70 cm (transversal walls of the ground floor) (see also Fig. 1).

4.2.2 Results in terms of effects on the pushover curves

Figure 20 illustrates the pushover curves obtained by the analyses in which also the out-of-plane contribution of piers have been accounted for; the results also refer to the hypothesis of perfect wall-to-wall connection.

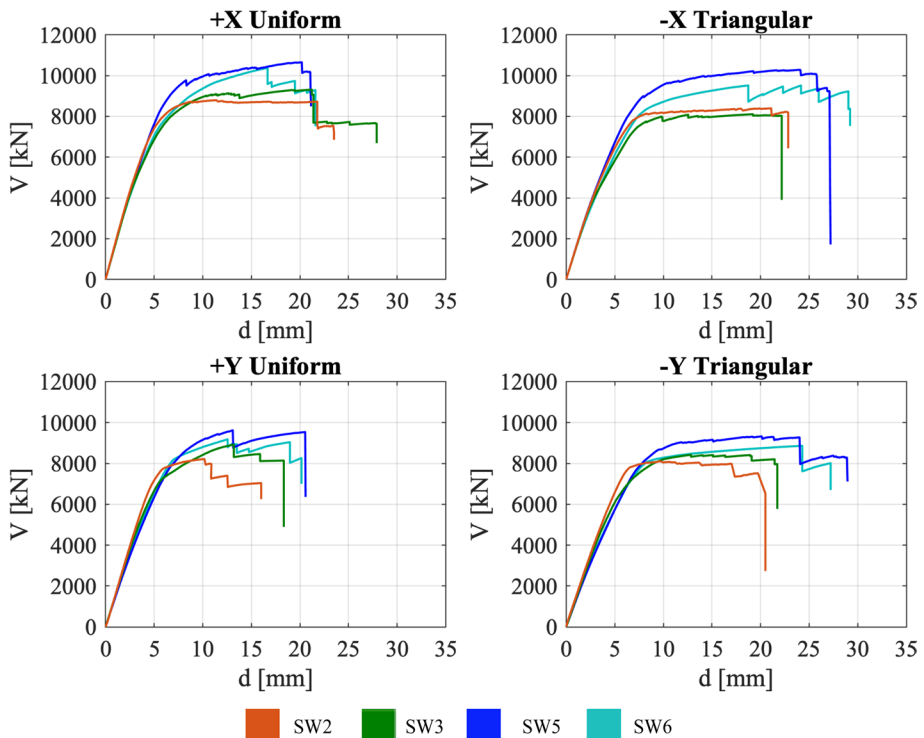


Fig. 20 Pushover curves resulting from the analyses in which the out-of-plane contribution is accounted for

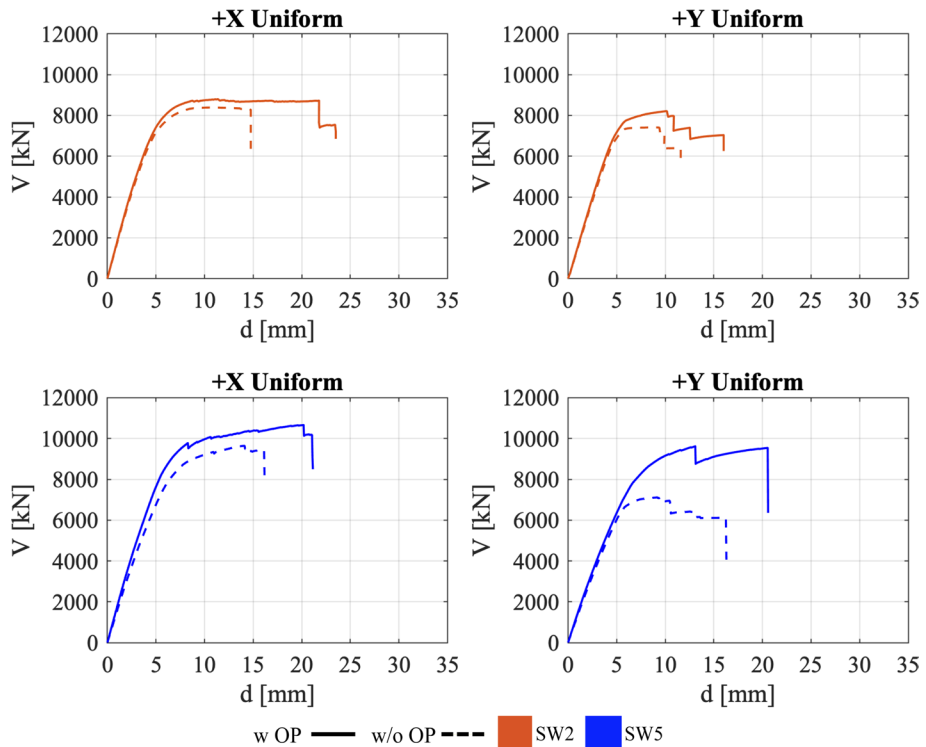


Fig. 21 Comparison of the capacity curves obtained with SW 2 and SW5 with (w OP) and without (w/o OP) the flexural out-of-plane contribution

In order to make more evident the effect of such a contribution, for two of the SWs, Fig. 21 directly compares the pushover curves obtained considering and neglecting the out-of-plane contribution (continuous and dashed lines, respectively). It is possible to observe an increase in the maximum strength and in the initial stiffness (although quite limited), as well as in the ultimate displacement capacity.

As introduced in Sect. 4.1, the flange (FE) and the out-of-plane (OP) effects are not completely decoupled, since both produce a variation in the acting axial load in the piers (altering the redistribution phenomena of the generalized forces). Thus, in order to understand such an interaction, the results associated to all the alternative combinations of possible hypotheses on these two modelling assumptions (namely: “w OP” or “w/o OP” and “w FE” or “w/o FE”, i.e. perfect or poor wall-to-wall connection) are reported in Fig. 22. As an example, the analyses were carried out only with SW2. Generally, the transition from “perfect” to “poor” wall-to-wall connection induces a reduction in the stiffness and overall base shear strength of the structure. Furthermore, it may be noted that, in the case of poor connection among the walls, a significant increase in the ultimate displacement capacity of the structure is observed.

It is worthy highlighting that in the general purpose software packages, where equivalent coupling beams with stiffness much greater than that of other structural elements have to be used to simulate the coupling effects, the execution of the pushover analyses requires

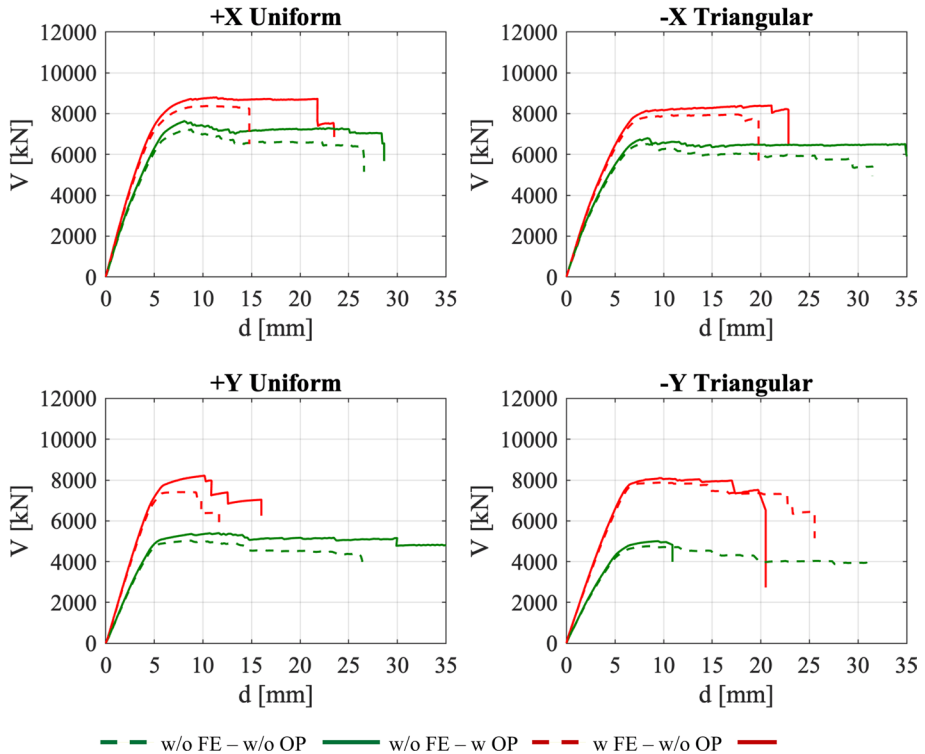


Fig. 22 Comparison of the pushover curves obtained with SW2 considering different combinations of the out-of-plane contribution (OP) and the flange effect (FE)

particular attention and a proper refinement in convergence other than additional calibration of the beams to correctly reproduce realistic failure mechanism and stable pushover curves.

4.3 Sensitivity to the adoption of alternative equivalent frame idealization criteria for URM walls

This section presents the results of some further investigations conducted with SW1 in order to evaluate the influence on the assessment of the seismic response of different possible assumptions for the pier effective height h_{eff} . To this aim, the possible alternative criteria already discussed in Sect. 2.1 have been adopted. Non-linear static analyses have been performed both in the positive and in the negative X and Y directions, assuming both the “uniform” and the “inverse triangular” load patterns. Figure 23 shows the comparison of the obtained results in terms of global pushover curves. As it can be seen, the different adopted hypotheses produce appreciable differences, in particular in terms of displacement capacity.

In order to quantify the dispersion associated to the obtained results, as already presented in Sect. 3.3, the percentage variation of the three parameters defining the equivalent bilinear curves has been computed. In particular:

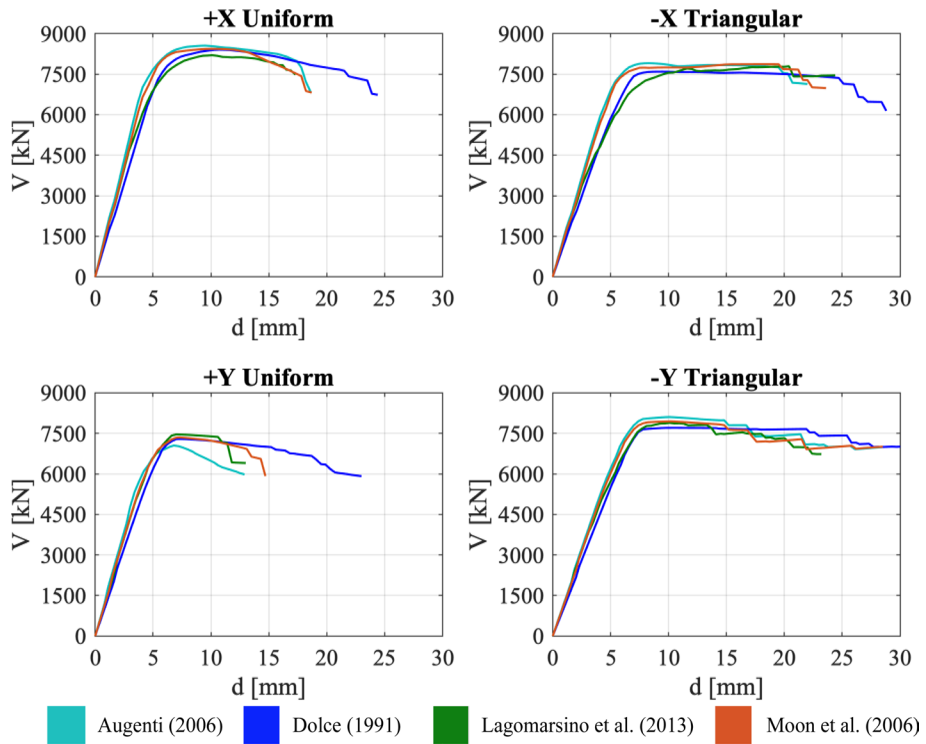


Fig. 23 Global pushover curves corresponding to the different adopted criteria for the EF idealization

- In Fig. 24 the percentage variation is computed assuming as reference the results obtained with the selected software package when the criterion of Lagomarsino et al. (2013) is adopted. This result quantifies the potential dispersion, being the same SW adopted for the analyses.
- In Fig. 25 the percentage variation is computed assuming as reference the average values resulting from all the six adopted SWs, as computed in Sect. 3.3 and reported in Table 5. In this case, the obtained scatter is affected not only by the uncertainty due to the criterion adopted for the definition of the geometrical dimensions of the structural elements of the EF model, but also by the intrinsic model uncertainty related to the choice of the software to use. This means, in other words, that the final dispersion is affected by the initial scatter characterizing the adopted software with respect to the “reference solution” (the one already highlighted in Sect. 3.3).

By looking at Figs. 24 and 25, it can be observed that the criterion proposed by Dolce (1991) in general lead to ultimate displacement capacities higher than the other ones, since it produces more slender piers (i.e. piers characterized by higher effective heights, see Figs. 3, 4 and 5) particularly subjected to a prevailing flexural response (which higher drift thresholds also correspond to). On the other hand, the four criteria

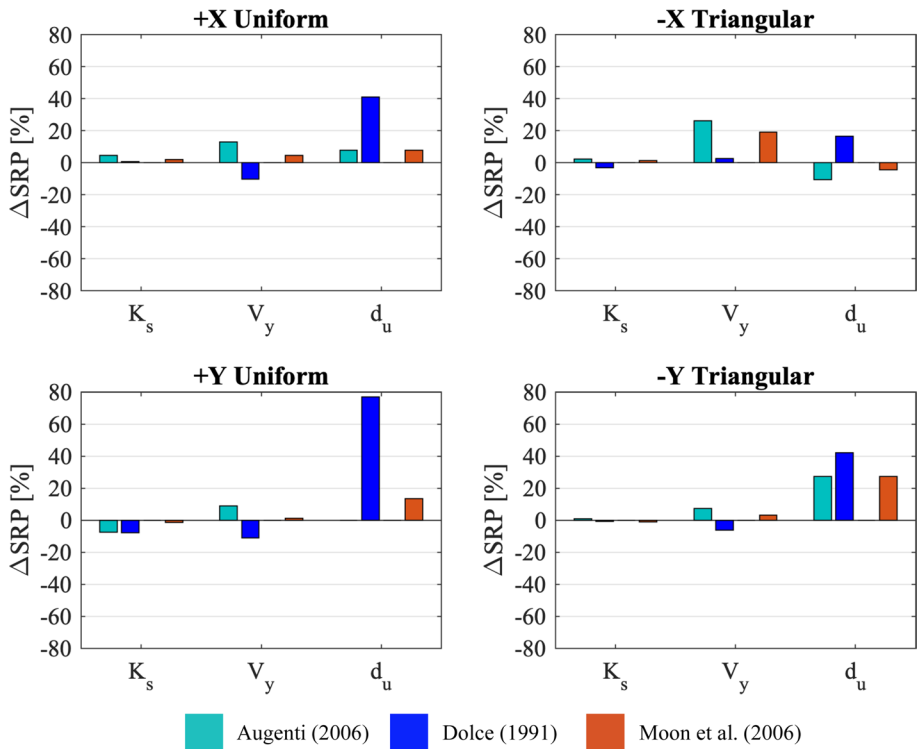


Fig. 24 Scatter with respect to solution of Lagomarsino et al. (2013) of the SRPs associated to the equivalent bi-linear curves (K_s , V_y and d_u): positive and negative direction of analysis

analyzed produce very similar responses in terms of overall base shear and stiffness, for both load patterns considered.

Further evidence on the potential influence of the adoption of alternative criteria for the EF idealization of walls are discussed in Manzini et al. (2021) for BS4 (2-storey single unit URM building).

5 Impact of the modelling uncertainties on the safety verification

5.1 Effect due to the software-to-software variability

The impacts on the safety verification of the dispersion of results analyzed in the previous sections are discussed in the following. To this aim, the comparison is herein made in terms of values of the maximum peak ground acceleration (PGA_{PL}) compatible with different performance levels (PL). In particular two PLs are considered, corresponding to the yield point of the equivalent bilinear curve (PGA_{V_y}) and to the ultimate displacement of pushover curves (PGA_{d_u}).

As an example, the results are reported with reference to case BS5/C and to the analyses carried out adopting the “uniform” load pattern.

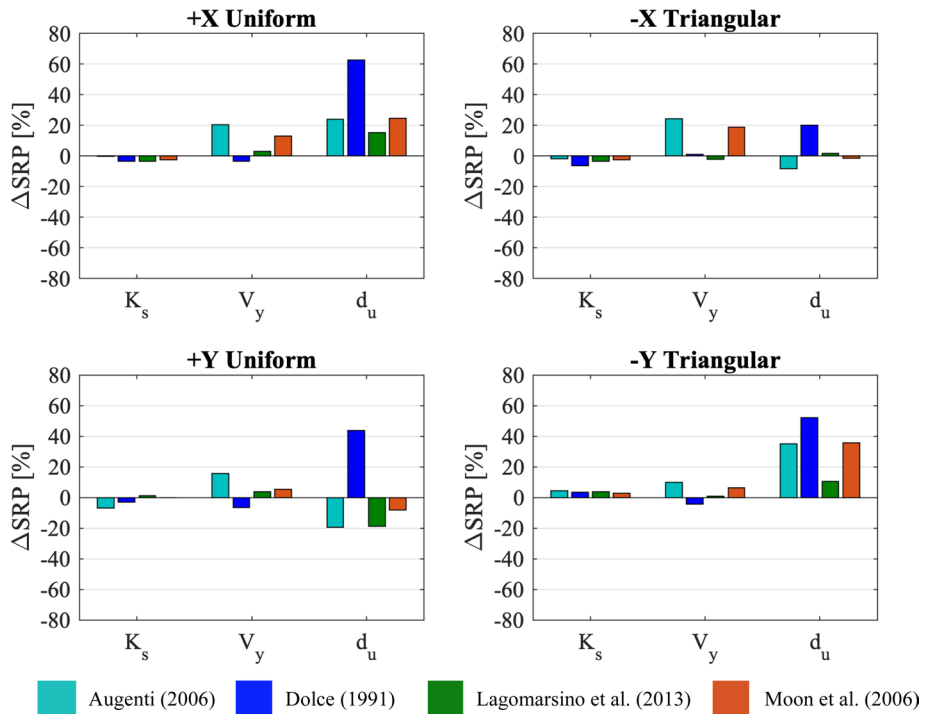


Fig. 25 Scatter with respect to the “benchmark solution” of the SRPs associated to the equivalent bi-linear curves (K_s , V_y and d_u): positive and negative direction of analysis

The N2 method (Fajfar 2000) has been adopted for the evaluation of the PGA. According to this method, the following differences among the results obtained through the SWs play a role in the final calculation of the PGA_{SL} :

- The values of the three parameters describing the equivalent bi-linear curve (F_y , K_s and d_u).
- The conversion factors (namely the participation factor Γ and participating mass m^*) addressed to convert the pushover curve representative of the MDOF into the equivalent SDOF system. In particular, these factors allow to convert the overall base shear and the stiffness into the yield acceleration ($A_y = F_y / \Gamma m^*$) and the equivalent T^* period, respectively.

According to the N2 method, the final value of PGA is also affected by the assumed value for T_c (i.e. the period that in the acceleration response spectrum separates the region at constant acceleration from that at constant velocity) and its relationship with T^* .

In particular, following data were used to calculate the spectral shape: soil factor $S = 1.52$; corner period $T_c = 0.714$; amplification factor $F_0 = 2.363$. These values are consistent with the seismic hazard of the Visso municipality, according to NTC (2018), for a return period of 475 years and the assumption of soil class D.

The following figures show the comparison of the values of the above-mentioned parameters obtained by the SWs. In particular, Fig. 25 reports the values of T^* : since the

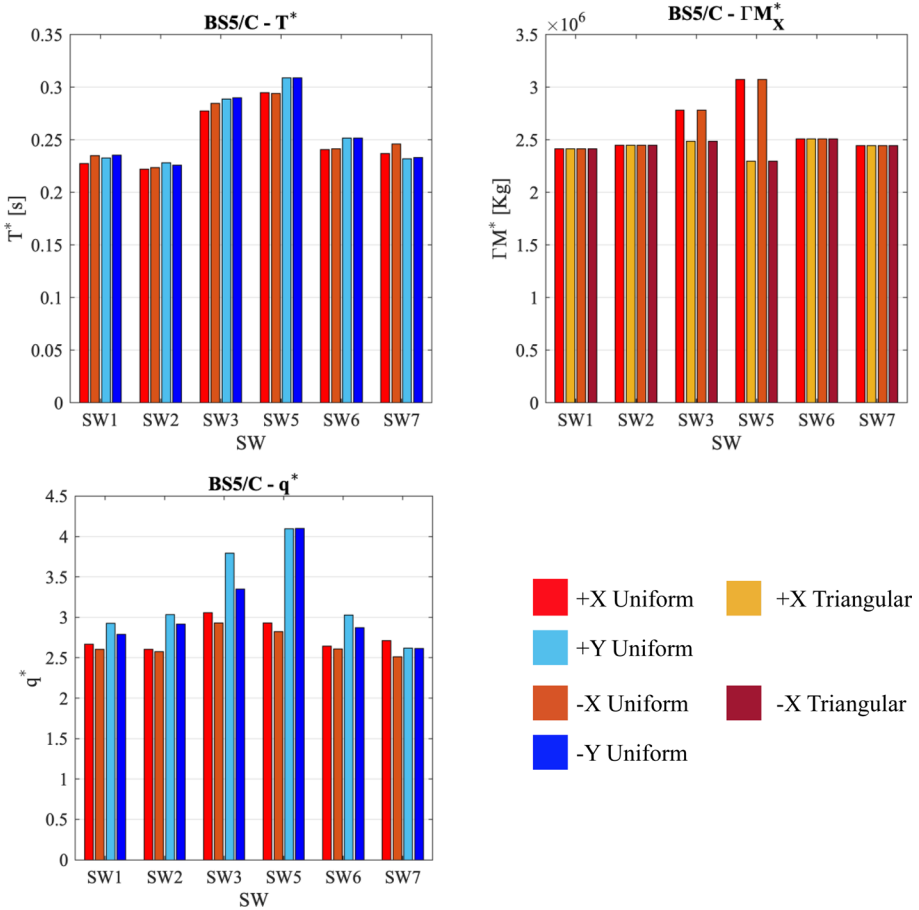


Fig. 26 T^* , ΓM^* , q^* values for different programs for both directions and load pattern

T^*/T_C ratio is lower than 1 for all cases, the calculation of the expected seismic demand is made with reference to the region of maximum amplification of the response spectrum. Moreover, the value of Γ is in most cases invariant with the load pattern (as shown in the product with m^* in Fig. 26, with reference in particular to the value of M_X^*). This is consistent with the assumption that the modal participation factor is calculated by most of the SWs referring to the eigenvector components of the first mode, regardless of the forces applied in the non-linear static analysis. Actually, in most of the commercial SWs used, the first mode is approximated by the deformed shape resulting from the application of the “triangular” load pattern on a linear elastic model of the structure. Few SWs allow to choose between different calculation methods for Γ . Conversely, in the case of SW3 and SW5, in the case of “uniform” load pattern the value of Γ is assumed unitary as default (without any alternative choice by the user).

Figure 27a shows the resulting values of PGA, while Fig. 27b illustrates the percentage variations with respect to the average value computed by considering the estimates provided by all the SWs. As it may be observed the variation results:

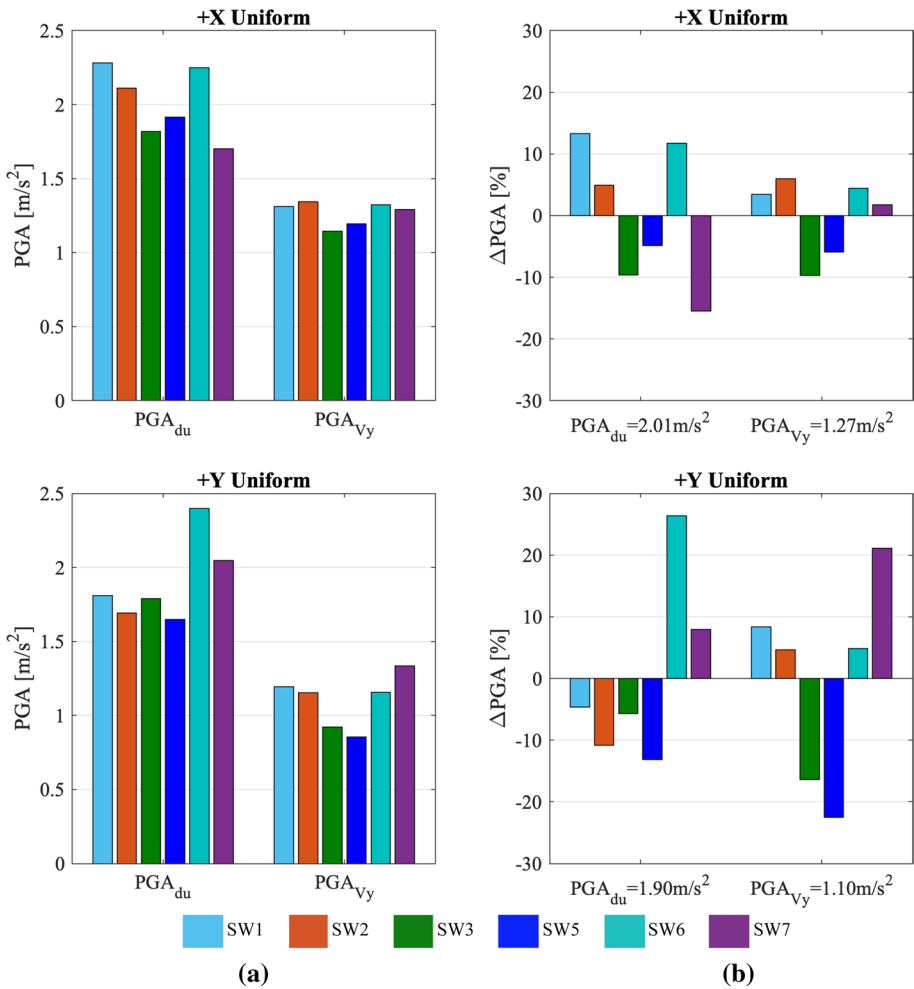


Fig. 27 PGA (a) and the scatter with respect to the average value (b) for the positive direction of analysis

- In the case of PGA_{Vy} : up to a maximum of 22% and on average 9%.
- In the case of PGA_{du} : up to a maximum of 26% and on average 10%.

The maximum values of these percentage variations occur in isolated cases, which typically refer to SW6 (in particular, for the PGA_{du} resulting from analysis in the Y direction), SW5 and SW7 (in particular, for the PGA_{Vy} always in the Y direction). The combined comparison of Fig. 27 with Fig. 8, reporting the percentage variations of the three parameters that define the equivalent bilinear curves, allows to verify that these latter results can be justified because of the greater differences found, in the case of SW6, in the ultimate displacement in the Y direction and, in the case of SW5 and SW7, in the overall base shear V_y and stiffness K_s , in the Y direction, with respect to the other SWs.

Table 7 Summary of the different modeling criteria adopted

Criteria	Percentage variations of PGA_{du} (%)											
	SW1		SW2		SW3		SW5		SW6		SW7	
	x	y	x	y	x	y	x	y	x	y	x	y
FE												
w	13	-5	5	-10	-10	-6	-5	-13	12	26	-15	8
w/o	-7	-13	31	15	-	-	-	-23	-36			
OP												
w	-	24	13	37	16	88	82	22	26	-		
w/o	13	-5	5	-10	-10	-6	-5	-13	12	26	-15	8
EF-I												
Augenti	26	-6	-	-	-	-	-					
Dolce	36	27	-	-	-	-	-					
Lagomarsino	13	-5	5	-10	-10	-6	-5	-13	12	26	-15	8
Moon	23	1	-	-	-	-	-					

- Not considered cases

5.2 Effect due to other alternative modelling options or modelling uncertainties

The computation of PGA_{du} has been repeated for all the cases examined in Sect. 4 considering different criteria for the EF idealization (EF-I) of the masonry walls, the out-of-plane contribution of piers (OP) and the effectiveness of the wall-to-wall connection (FE). The obtained results are summarized in Table 7, where the percentage variations of PGA_{du} are always computed with respect to the “average solution” reported in Sect. 5.1 referring to results obtained in Sect. 3. Considering the different modelling uncertainties, for SW1 the different criteria for the EF idealization brings a greater variation of PGA_{du} than the wall-to-wall connection. In the case of SW2, the out-of-plane contribution and the wall-to-wall connection led to very similar variations. In general, as expected, to consider the out-of-plane contribution causes greater values of PGA , particularly for SW5. Figure 28 also summarizes the corresponding PGA_{du} values and shows that a greater variation among the different criteria for the EF idealization results for PGA_{du} than for PGA_{Vy} , highlighting how the different idealization affects especially the ultimate displacement.

6 Conclusions

The paper presents the results obtained within the research activity carried out by several research teams involved in the “*URM nonlinear modelling—Benchmark project*” on the benchmark structure BS5, inspired by the “P. Capuzi” school in Visso (MC, Italy).

The benchmark structure has been analyzed by exploring the influence of different modelling assumptions, aimed to reflect those most commonly adopted by analysts at both research and professional levels. Nonlinear static analyses have been performed by SWs, also available at commercial level. Although not exhaustive, the considered set of SWs reflects the tools available to professionals in Italy nowadays; moreover, many of the selected SWs are used also at international level. In that way, it is expected that the

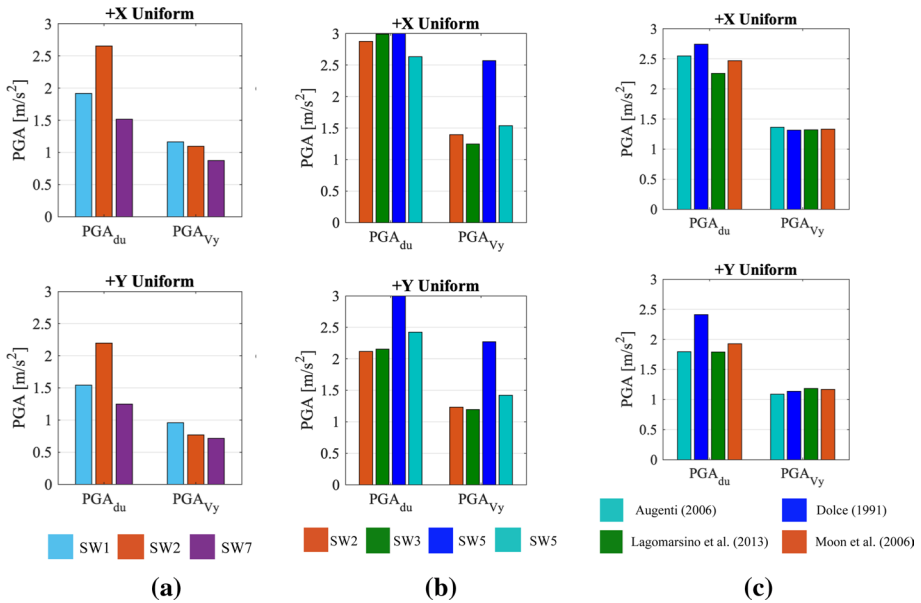


Fig. 28 PGA_{du} values obtained for the conditions examined: **a** low wall-to-wall connection; **b** contribution of the out-of-plane of the piers; **c** EF idealization (SW1)

quantification of the dispersion on achievable results discussed in the paper will constitute a useful reference for the scientific community and professional engineers as well.

The comparison of the obtained results covers a large set of parameters related to: dynamic properties of the buildings; pushover curves (also described by three synthetic parameters when passing to their equivalent bilinear curves); damage pattern; indicators useful for the safety verification aims.

With respect to other comparative studies available in the literature (as examined in detail in Cattari and Magenes 2021 and mentioned in the introduction), the results confirm that the dispersion achievable when different software packages are used is not completely negligible, as already shown by the analysis of other benchmark structures (like as in Manzini et al. 2021; Degli Abbati et al. 2021). Moreover, the configuration associated to “weak-spandrels” tends to produce higher dispersion values (at least in the initial stiffness and overall base shear) than that in which spandrels are coupled to other tensile resistant elements. However, on the other hand, the dispersion is contained within acceptable values if the consistency on the modelling assumptions across the EF models is carefully checked and guaranteed.

Acknowledgements The study presented in the paper was developed within the research activities carried out in the frame of the 2014–2018 ReLUI Project (Topic: Masonry Structures; Coord. Proff. Sergio Lagomarsino, Guido Magenes, Claudio Modena, Francesca da Porto) and of the 2019–2021 ReLUI Project—WP10 “Code contributions relating to existing masonry structures” (Coord. Guido Magenes). The projects are funded by the Italian Department of Civil Protection. Moreover, the Authors acknowledge the following members of research teams (RT) that participated to the analyses of the benchmark structure illustrated in this paper or in his companion paper: UniPV RT (University of Pavia: Coord. Guido Magenes, Participants: Paolo Morandi); UniCH RT (University of Chieti-Pescara: Coord. Prof. Guido Camata); UniCT RT (University of Catania: Coord. Prof. Ivo Calì, Participants: Francesco Canizzaro, Giuseppe Occhipinti, Bartolomeo Pantò); UniNA RT (University Federico II of Naples: Coord. Prof. Bruno Calderoni, Participants:

Gaetana Pacella, Carmen Cafero, Lucia Di Sarno); UniBO RT (University of Bologna: Coord. Prof. Stefano de Miranda, Participants: Giovanni Castellazzi, Antonio Maria D’Altri); POLIMI RT (Polytechnic of Milan: Coord. Prof. Gabriele Milani); IUAV RT (University of Venice: Coord. Prof. Anna Saetta, Participants: Luisa Berto, Diego Alejandro Talledo).

Authors’ contributions DO: data curation, numerical analyses, comparisons of results made by the research teams, writing-original draft; CFM: numerical analyses, interpretation of results, writing-review; CM: numerical analyses, interpretation of results, writing-review; EAC: numerical analyses, writing-review; SC: conceptualization, methodology, interpretation of results, supervision, writing-review.

Funding Open access funding provided by Università degli Studi di Genova within the CRUI-CARE Agreement. The research activity “*URM nonlinear modelling—Benchmark project*”, whose methodology and benchmark structures proposed, are presented in this paper, did not receive any grant from funding agencies in the public, commercial or not-for-profit sectors that may gain or lose financially through publication of this work.

Availability of data and material The benchmark structure analysed in the paper (BS5) can be replicated by other researchers and analysts thanks to the input data provided in the paper by Cattari and Magenes (2021) as supplementary electronic material (Annex I-*Benchmark Structures Input Data*). Some additional data support the findings of this study are available from the corresponding author upon reasonable request.

Declarations

Conflict of interest The authors declare that they have no known competing financial interests or personal relationships that could have appeared to influence the work reported in this paper.

Open Access This article is licensed under a Creative Commons Attribution 4.0 International License, which permits use, sharing, adaptation, distribution and reproduction in any medium or format, as long as you give appropriate credit to the original author(s) and the source, provide a link to the Creative Commons licence, and indicate if changes were made. The images or other third party material in this article are included in the article’s Creative Commons licence, unless indicated otherwise in a credit line to the material. If material is not included in the article’s Creative Commons licence and your intended use is not permitted by statutory regulation or exceeds the permitted use, you will need to obtain permission directly from the copyright holder. To view a copy of this licence, visit <http://creativecommons.org/licenses/by/4.0/>.

References

- 2Si (2020) PRO_SAM Program, included in PRO_SAP Program, Release 20.7.0, www.2si.it/en/pro_sam_eng/3Muri Program (2016) Release 11.0., distributed by STADATA. www.3muri.com.
- Aedes PCM (2017) Progettazione di Costruzioni in Muratura, Release 2017.1.4.0 distributed by Aedes, Manuale d’uso (in Italian)
- ASCE 41-17 (2017) Seismic evaluation and upgrade of existing buildings, American Society of Civil Engineers, Reston, Virginia
- Aşıkoğlu A, Vasconcelos G, Lourenço PB, Pantò B (2020) Pushover analysis of unreinforced irregular masonry buildings: Lessons from different modeling approaches. *Eng Struct*. <https://doi.org/10.1016/j.engstruct.2020.110830>
- Aşıkoğlu A, Vasconcelos G, Lourenço PB (2021) Overview on the nonlinear static procedures and performance-based approach on modern unreinforced masonry buildings with structural irregularity. *Buildings* 11:147. <https://doi.org/10.3390/buildings11040147>
- Augenti N (2006) Seismic behavior of irregular masonry walls. In: 1st European conference on earthquake engineering and seismology, Geneva, Switzerland
- Azizi-Bondarabadi H, Mendes N, Lourenço PB (2019) Higher mode effects in pushover analysis of irregular masonry buildings. *J Earthq Eng*. <https://doi.org/10.1080/13632469.2019.1579770>
- Bartoli G, Betti M, Biagini P, Borghini A, Ciavattone A, Girardi M, Lancioni G, Marra AM, Ortolani B, Pintucchi B, Salvatori L (2017) (2017) Epistemic uncertainties in structural modeling: a blind benchmark for seismic assessment of slender masonry towers. *J Perform Constr Facil* 31(5):04017067

- Berti M, Salvatori L, Orlando M, Spinelli P (2017) Unreinforced masonry walls with irregular opening layouts: reliability of equivalent-frame modelling for seismic vulnerability assessment. *Bull Earthq Eng* 15(3):1213–1239
- Betti M, Galano L, Vignoli A (2008) Seismic response of masonry plane walls: a numerical study on spandrels strength. *AIP Conf Proc* 1020:787. <https://doi.org/10.1063/1.2963915>
- Betti M, Galano L, Vignoli A (2014) Comparative analysis on the seismic behaviour of unreinforced masonry buildings with flexible diaphragms. *Eng Struct* 61:195–208
- Beyer K, Mangalathu S (2013) Review of strength models for masonry spandrels. *Bull Earthq Eng* 11:521–542
- Bracchi S, Rota M, Penna A, Magenes G (2015) Consideration of modelling uncertainties in the seismic assessment of masonry buildings by equivalent-frame approach. *Bull Earthq Eng* 13:3423–3448
- Brunelli A, de Silva F, Piro A, Parisi F, Sica S, Silvestri F, Cattari S (2021) Numerical simulation of the seismic response and soil-structure interaction for a monitored masonry school building damaged by the 2016 Central Italy earthquake. *Bull Earthq Eng* 19(2):1181–1211. <https://doi.org/10.1007/s10518-020-00980-3>
- Calderini C, Cattari S, Lagomarsino S (2009) In-plane strength of unreinforced masonry piers. *Earthq Eng Struct Dyn* 38(2):243–267
- Calderoni B, Cordasco EA, Sandoli A, Onotri V, Tortoriello G (2015) Problematichette di modellazione strutturale di edifici in muratura esistenti soggetti ad azioni sismiche in relazione all'utilizzo di software commerciali. In: Proceedings of XVI ANIDIS conference. 13–17 Settembre, L'Aquila, Italia. (In Italian)
- Castellazzi G, Pantò B, Occhipinti G, Talledo DA, Berto L, Camata G (2021) A comparative study on a complex URM building. Part II: issues on modelling and seismic analysis through continuum and discrete-macroelement models. *Bull Earthquake Eng*, SI on URM non modelling—Benchmark Project, under review
- Cattari S, Magenes G (2021) Benchmarking the software packages to model and assess the seismic response of URM existing buildings through nonlinear static analyses. *Bull Earthq Eng*. <https://doi.org/10.1007/s10518-021-01078-0>
- Cattari S, Calderoni B, Caliò I, Camata G, Cattari S, de Miranda S, Magenes G, Milani G, Saetta A (2021a) Nonlinear modelling of the seismic response of masonry structures: critical aspects in engineering practice. *Bull Earthquake Eng*, SI on URM non modelling—Benchmark Project, under review
- Cattari S, Camilletti D, D'Altri AM, Lagomarsino S (2021b) On the use of continuum Finite Element and Equivalent Frame models for the seismic assessment of masonry walls. *J Build Eng* 43:102519. <https://doi.org/10.1016/j.jobbe.2021.102519>
- Cattari S, Degli Abbati S, Ottonelli D, Marano C, Camata G, Spacone E, da Porto F, Modena C, Lorenzoni F, Magenes G, Penna A, Graziotti F, Ceravolo R, Miraglia G, Lenticchia E, Fiorini N, Spina D (2019) Discussion on data recorded by the Italian structural seismic monitoring network on three masonry structures hit by the 2016–2017 Central Italy earthquake. *COMPdyn*, 24–26 June 2019, Crete, Greece CDSWin (2016) distributed by STS s.r.l. www.stsweb.it/prodotto/ti/strutturali/cdswin
- CEN 2005. Eurocode 8. Design provisions for earthquake resistance of structures. Part 3: Assessment and retrofitting of buildings. Brussels, Belgium: CEN (European Committee for Standardization); 2005.
- D'Altri AM, Cannizzaro F, Petracca M, Talledo DA (2021) Nonlinear modelling of the seismic response of masonry structures: calibration strategies. *Bull Earthq Eng*. <https://doi.org/10.1007/s10518-021-01104-1>
- De Falco A, Guidetti G, Mori M, Sevieri G (2017) Model uncertainties in seismic analysis of existing masonry buildings: the Equivalent-Frame Model within the Structural Element Models approach. In: Proceedings of XVII ANIDIS conference, 17–21 Settembre, Pistoia, Italia. (in Italian)
- Degli Abbati S, Morandi P, Cattari S, Spacone E (2021) On the reliability of the equivalent frame models: the case study of the permanently monitored Pizzoli's town hall. *Bull Earthquake Eng*, SI on “URM nonlinear modelling—Benchmark Project”, under review
- Dolce M, Nicoletti M, De Sortis A, Marchesini S, Spina D, Talanas F (2017) Osservatorio sismico delle strutture: the Italian structural seismic monitoring network. *Bull Earthq Eng* 15(2):621–641
- Dolce M (1991) Schematizzazione e modellazione degli edifici in muratura soggetti ad azioni sismiche. *L'industria Delle Costruzioni* 25(242):44–57
- Esposito R, Messali F, Ravenshorst GJP, Shipper HR, Rots JG (2019) (2019) Seismic assessment of a lab-tested two-storey unreinforced masonry Dutch terraced house. *Bull Earthq Eng* 17:4601–4623
- Fajfar P (2000) A nonlinear analysis method for performance-based seismic design. *Earthq Spectra* 16(3):573–592. <https://doi.org/10.1193/1.1586128>

- Ferrero C, Lourenco PB, Calderini C (2020) Nonlinear modeling of unreinforced masonry structures under seismic actions: validation using a building hit by the 2016 Central Italy earthquake. *Frattura Ed Integrità Strutturale* 14(51):92–114
- Giamundo V, Sarhosis V, Lignola GP, Sheng Y, Manfredi G (2014) Evaluation of different computational modelling strategies for the analysis of low strength masonry structures. *Eng Struct* 73:160–169
- Graziotti F, Toninelli P, Solenghi M, Guerrini G, Penna A (2019) Numerical simulation of the earthquake response of a monitored URM school building. *COMPdyn*, 24–26 June 2019, Crete, Greece
- Kržan M, Gostič S, Cattari S, Bosiljkov V (2015) Acquiring reference parameters of masonry for the structural performance analysis of historical buildings. *Bull Earthq Eng* 13(1):203–236
- Lagomarsino S, Penna A, Galasco A, Cattari S (2013) TREMURI program: an equivalent frame model for the nonlinear seismic analysis of masonry buildings. *Eng Struct* 56:1787–1799. <https://doi.org/10.1016/j.engstruct.2013.08.002>
- Magenes G, Manzini CF, Morandi P (2006) SAM-II, Software for the Simplified Seismic Analysis of Masonry buildings, Università degli Studi di Pavia and EUCENTRE
- Manzini CF, Morandi P, Magenes G, Calliari R (2006) ANDILWall Program, Release 3.1.0.0—Software di calcolo e verifica di edifici in muratura ordinaria, armata o mista—Manuale d’uso (in Italian), Università di Pavia, EUCENTRE and CRSoft, www.andilwall.it
- Manzini CF, Ottonelli D, Degli Abbatì S, Marano C, Cordasco EA (2021) Modelling the seismic response of a 2-storey URM benchmark case study: comparison among different equivalent frame models. *Bull Earthq Eng (SI on “URM nonlinear modelling—Benchmark Project”)*
- Marques R, Lourenço PB (2011) Possibilities and comparison of structural component models for the seismic assessment of modern unreinforced masonry buildings. *Comput Struct* 89(21–22):2079–2091
- Marques R, Lourenço PB (2014) Unreinforced and confined masonry buildings in seismic regions: validation of macro-element models and cost analysis. *Eng Struct* 64:52–67
- Mendes N, Costa AA, Lourenço PB, Bento R, Beyer K, de Felice G, Gams M, Griffith M, Ingham JM, Lagomarsino S, Lemos JV, Liberatore D, Modena C, Oliveira DV, Penna A, Sorrentino L (2017) Methods and approaches for blind test predictions of out of-plane behavior of masonry walls: a numerical comparative study. *Int J Arch Herit* 11(1):59–71
- MIT (2019) Ministry of Infrastructures and Transportation, Circ. C.S.LI.PP. No. 7 of 21/1/2019. Istruzioni per l’applicazione dell’aggiornamento delle norme tecniche per le costruzioni di cui al Decreto Ministeriale 17 Gennaio 2018. G.U. S.O. n.35 of 11/2/2019 (in Italian)
- MIDAS Gen® (2017) MIDAS Information Technology Co., <http://en.midasuser.com>, www.cspfea.net
- Moon FL, Yi T, Leon RT, Kahn LF (2006) Recommendations for seismic evaluation and retrofit of low-rise URM structures. *J Struct Eng* 132(5):663–672
- NTC (2018) Italian Technical Code, Decreto Ministeriale 17/1/2018. Aggiornamento delle Norme tecniche per le costruzioni. Ministry of Infrastructures and Transportation, G.U. n.42 of 20/2/2018 (in Italian)
- Parisi F, Augenti N (2013) Seismic capacity of irregular unreinforced masonry walls with openings. *Earthq Eng Struct Dyn* 42:101–121
- Parisse F, Cattari S, Marques R, Lourenco PB, Magenes G et al (2021) Benchmarking the seismic assessment of unreinforced masonry buildings from a blind prediction test. *Structures*. <https://doi.org/10.1016/j.istruc.2021.01.096>
- Quagliarini E, Maracchini G, Clementi F (2017) Uses and limits of the equivalent frame model on existing unreinforced masonry buildings for assessing their seismic risk: a review. *J Build Eng* 10:166–182
- Rota M, Penna A, Magenes G (2014) A framework for the seismic assessment of existing masonry buildings accounting for different sources of uncertainty. *Earthq Eng Struct Dyn* 43(7):1045–1066
- SAP 2000 (2016) Release 18, distributed by Computers and Structures Inc., www.csiam.eric.com/products/sap2000
- Salonikios T, Karakostas C, Lekidis V, Anthoine A (2003) Comparative inelastic pushover analysis of masonry frames. *Eng Struct* 25:1515–1523
- Siano R, Roca P, Camata G, Pelà L, Sepe V, Spacone E, Petracca M (2018) Numerical investigation of nonlinear equivalent-frame models for regular masonry walls. *Eng Struct* 173:512–529
- Spacone E, Camata G (2007) Cerniere Plastiche sviluppate per telai in cemento armato e implementate nel programma di calcolo Aedes (in Italian), Issued by GC, Ottobre 2007
- Turnšek V, Čačovič F (1971) Some experimental results on the strength of brick masonry walls. In: Proceedings of the 2nd international brick masonry conference, stoke-on-trent, 1970. pp 149–156
- Turnsek V, Sheppard P (1980) The shear and flexural resistance of masonry walls. In: Proceedings of international research conference on earthquake engineering, Skopje, 1980
- Vanin F, Zaganelli D, Penna A, Beyer K (2017) Estimates for the stiffness, strength and drift capacity of stone masonry walls based on 123 quasi-static cyclic tests reported in the literature. *Bull Earthq Eng* 15(12):5435–5479

Publisher's Note Springer Nature remains neutral with regard to jurisdictional claims in published maps and institutional affiliations.

Authors and Affiliations

Daria Ottonelli¹ · Carlo Filippo Manzini² · Corrado Marano³ · Emilia Angela Cordasco⁴ · Serena Cattari¹ 

¹ Department of Civil, Chemical and Environmental Engineering, University of Genoa, Genoa, Italy

² Department of Construction and Infrastructure, EUCENTRE Foundation, Pavia, Italy

³ Department of Engineering and Geology, University of Chieti-Pescara, Chieti, Italy

⁴ Department of Structural Engineering, University of Napoli, Napoli, Italy